

# *APPLE, ATOMIC PLANAR POWER FOR LIGHTWEIGHT EXPLORATION*

NIAC PHASE I FINAL REPORT

January 11, 2022

**E. Joseph Nemanick**, The Aerospace Corporation, Energy Technology Department  
**Henry Helvajian**, The Aerospace Corporation, Surface Science & Engineering Department  
**Gabriel Veith**, Oak Ridge National Laboratories, Chemical Sciences Division  
**Kristine Ferrone**, The Aerospace Corporation, Space Sciences Department  
**Adon Delgado**, The Aerospace Corporation, Thermal Control Department

Prepared for:

NASA Innovative Advanced Concepts  
NASA Space Technology Mission Directorate  
300 E. St. SW  
Washington, DC 20546

Solicitation No. 80HQTR20NOA01-21NIAC-A1



## Executive Summary

The *Atomic Planar Power for Lightweight Exploration* (APPLE) is a low mass, high reliability spacecraft power architecture that merges the extensive heritage of radioisotope power generation with a radiation-hard battery in a robust modular system which can enable a wide range of spacecraft and rover design. The Phase I APPLE design consists of a radiation hard battery serving the dual role of power storage and thermal radiation interface on top of which are placed multiple power source “cores” (1 x 1 x 1.7 cm modules) are tiles of  $^{238}\text{PuO}_2$  mated to thermoelectric couples. Four cores are located in a 10 cm x 10 cm tile with an integral radiation hard battery layer. The primary Phase I findings are:

- The APPLE architecture is not only feasible but also opens the design space for spacecraft and mission designs through distributed power that scales across vehicle sizes, from 10's of Watts to kilowatt systems.
- Thermal simulations showed that locating the battery at the thermoelectric cold shoe/radiator junction maintains a temperature range between 60°C and 140°C for the battery while the hot shoe thermoelectric junction remains at 527°C.
- Modelling of the radiation dose and capture depth indicates that  $^{238}\text{PuO}_2$  is the optimal heat source for APPLE, with no need for radiation shielding for the battery.
- Radiation simulations of the mission environment indicate that galactic cosmic radiation and solar flares are the dominant radiation exposure sources for a vehicle in transit.

In Phase I, the APPLE design underwent several design changes as a result of the simulations of the isotope/thermoelectric interface, the thermal profile, and radiation exposure/capture modeling. It was discovered that limiting the isotope temperature to the maximum theoretical battery compatible temperature (400°C) negatively impacted the battery capacity and calendar life by eliminating high performing battery materials. In addition, limiting the isotope/thermoelectric interface (“hot shoe”) temperature reduced thermoelectric conversion efficiency and the usable types of thermoelectric materials. An innovative solution was discovered where the radiation hard battery serves as the thermal radiator, locating the battery on the cold shoe, permitting the hot shoe temperature to float and opening the design space for both battery and thermoelectric material choices. In the proposed configuration the battery temperature ranges between 60-140°C. Analyses show that within this temperature range the battery design can be more energy dense by using lithium metal anodes, and use high capacity layered lithium ion cathodes. Moreover, in this temperature range, the solid state electrolyte shows optimal ionic conductance and calendar life. In addition, the large surface area of the battery radiator substantially increased (37%) the thermoelectric efficiency without adding mass. APPLE is intended to utilize waste heat from the isotope to reduce the need for component heaters and power. In Phase I, thermal analysis was performed showing that the residual thermal energy for warming the spacecraft bus and/or payload components could be extracted without negatively impacting thermoelectric conversion efficiency.

The Phase I radiation simulation studies show that the isotope junction is free from substantial ionizing radiation from  $^{238}\text{PuO}_2$  due to the short penetration depth of its alpha particle radiation. However, other isotope sources ( $^{90}\text{Sr}$  and  $^{241}\text{Am}$ ) show longer penetration lengths that would need to be accounted for if those isotope sources were used. As a power architecture, APPLE still takes on significant radiation exposure over mission life (15+ years) from both galactic cosmic background radiation, as well as solar flare particles. For the battery portion, these ionizing particles were projected to induce exposure in the range from 10 to 50 Gy.

## Contents

<b>I. Executive Summary</b>	<b>i</b>
<b>1. Concept Overview</b>	<b>1</b>
1.1. Motivation	2
1.2. RTG Requirements	3
1.3. Current Battery Capability	4
1.4. Technology Needs	6
<b>2. Radiation Simulations</b>	<b>7</b>
2.1. Radioisotope Selection	7
2.2. Methodology and Results	9
2.3. Solar and Galactic Radiation Exposure	10
2.4. Calculated Battery Radiation Dose	11
2.5. Translation of Dose Equivalent to Dose	13
2.6. Mission Applications	13
2.7. Next Steps in Phase II	14
<b>3. Battery Design and Testing</b>	<b>15</b>
3.1. Need for a Solid State, Radiation Hard Battery	15
3.2. Solid State Radiation Hard Battery Fabrication	15
3.3. Electrochemical Activation and Testing	17
3.4. Radiation Testing of Cells	18
3.5. Next Steps in Phase II	20
<b>4. Thermal Design Simulations</b>	<b>21</b>
4.1. Introduction	21
4.2. Isotope Properties	23
4.3. Thermoelectric Design Considerations	23
4.4. PATRAN Thermal Simulations	26
4.5. Next Steps in Phase II	32
<b>5. Mission and Application</b>	<b>34</b>
5.1. Introduction	34
5.2. APPLE Tile Designs	34
5.3. APPLE Powering the Solar Gravity Lens Mission	35
5.4. Direct Spacecraft Thermal Regulation through APPLE	37
5.5. APPLE Antenna Structures	38
5.6. APPLE Powered Ingenuity Follow On	39
<b>6. APPLE Development Path</b>	<b>40</b>
6.1. Isotope Supply	40
6.2. APPLE Thermal Core Framework	41
6.3. APPLE Power and Mass Designs	41
6.4. Launch Safety	45
6.5. Spacecraft Cooling Needs	45
6.6. Phase II Project Plan	46
<b>7. References</b>	<b>47</b>

*The Atomic Planar Power for Lightweight Exploration, (APPLE), is an enabling architecture for solar system exploration with low mass vehicles. Its goal is to develop an advanced vehicle power architecture that integrates lightweight radioisotope power with robust, radiation hard energy storage in a modular, scalable power system.*

## 1. Concept Overview

APPLE is a radioisotope-based modular power and energy storage spacecraft architecture that enables long duration missions destined for the outer reaches of the solar system. In these regions solar photon flux is nil, requiring radioisotope power sources. However, peak power requirements for some missions are high, requiring robust energy storage. Finally, both power and energy storage systems must be long lived and durable. This power system can enable fast-transit spacecraft missions by providing a substantially lower mass power system architecture than conventional RTGs and batteries, while still providing long mission life (30+ years). It can also power small planetary rovers where the existing large RTGs are too large. The architecture will drive rapid exploration of the deepest parts of the Solar System via a low mass power system architecture. This will enable scientific exploration on smaller (e.g. nanosatellite class) spacecraft, unlocks the use of solar sail propulsion for increased vehicle velocity to send nanosatellite class vehicles distant locations, and opens up RTG power for small rovers, and accelerates vehicle and mission design through a modular power system.

The **Atomic Planar Power for Lightweight Exploration (APPLE)** is a low mass, high reliability spacecraft power architecture that merges the extensive heritage of radioisotope power generation with a radiation-hard battery in an integrated modular system which can enable a wide range of vehicle and mission designs. A modular power architecture will open up the design space for spacecraft bus by enabling power designs to fit the mission for any vehicle shape or size, from 10's of Watts to kilowatts. As shown in Figure 1 APPLE uses small  $^{238}\text{PuO}_2$  tiles coupled to high efficiency thermoelectric devices joined to a thermal radiator that also serves as a 5 Wh solid state radiation hard battery in a 10 x 10 x 1.7 cm tile. The current design device is estimated to produce at least 1.2 W<sub>e</sub> before design optimization and last at least 15 years ( $^{238}\text{Pu}$  half-life is 87.7 years). Moreover, in addition to power generation this power tile

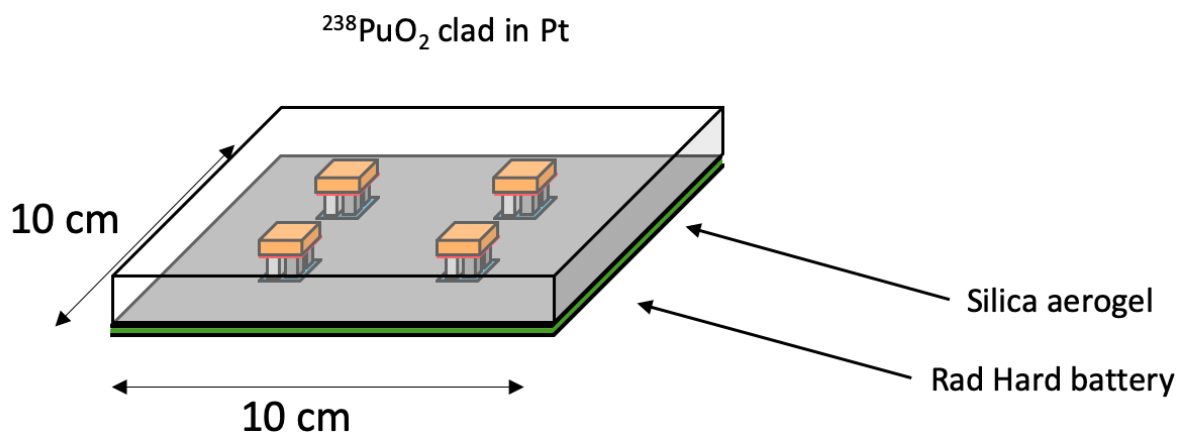


Figure 1. An APPLE single sided tile. The battery serves a dual function role energy storage/radiator. The tile comprises multiple distributed thermal Cores that include the thermoelectric energy conversion. Analysis shows that a 10 cm x 10 cm tile should produce ~1.2 W<sub>e</sub> at the end of a 15 year mission while providing 5 Wh energy storage. Two single sided tiles mated back-to-back would form a double sided tile with twice the capability.

can be placed on the vehicle surface to provide heat for internal components or in a dual sided configuration on a boom-type extension to provide more power ( $\sim 2 \text{ W}_e/\text{tile}$ ).

Current chemical propulsion technologies reach 3-5 AU/yr velocities for spacecraft. For spacecraft with higher transit velocities ( $>15 \text{ AU/yr}$ ) which can be achieved via solar sails<sup>1</sup> propulsion and a close solar perihelion transit, it is essential that the total vehicle mass be low while retaining high power capability and reliability of the avionics and payloads. For a practical solar sail area, this forces the total spacecraft mass to be within 10-20 kg for transit velocities of 10-20 AU/yr. Even for nanosatellites ( $\sim 10 \text{ kg}$ ) with electric propulsion,<sup>2</sup> a power system mass less than 1-2 kg would be a mission enabler. Whatever the propulsion source, existing qualified RTG systems are massive, constant power systems, and designed only for large vehicles. In addition, conventional battery technology requires shielding from radiation and particulates from the space environment limiting their placement to deep interior of vehicles. Many current and next generation deep space mission designs like Solar Gravity Lens, SIMPLEx, and MarCO use low mass vehicles that cannot accommodate large RTGs or spare excess mass for power system shielding. Without onboard, small size, robust power sources their power would have to be supplied through energy beaming or short lived primary batteries further limiting capability and increasing vehicle mass. Consequently, the APPLE power system architecture fills a key technology gap. A modular and scalable RTG + battery technology would allow for design flexibility and enable deep space small vehicle missions. This technology gap is addressed by the modular nature of the APPLE architecture providing power, storage, and heating.

Current power systems for small planetary rovers are limited to either photovoltaic systems or primary batteries. While MSL and Curiosity are RTG powered, these are large (900 kg) vehicles. Smaller vehicles like those needed for more distant destinations (Enceladus, Europa, Titan), or for novel propulsion systems (helicopters, swimmers, climbers) need a small, capable power system. The existing RTG systems are simply too massive for deployment on small (10-20 kg) vehicles. To open up planetary rover exploration, a lightweight power system is needed that does not depend sunlight. In addition, these destinations often have challenging thermal environments (heat sapping convective atmospheres) and existing battery technologies have delicate thermal constraints that require significant heater power. A small power system that utilizes its own heat can reduce rover mass while extending exploration and science.

This Phase I work demonstrated the radiation environment internal to APPLE from the isotope source as well as the radiation environment from external sources such as galactic cosmic radiation and solar particles. This work also began radiation hard solid state battery fabrication and electrochemical and radiation testing. This project also undertook thermal optimization for APPLE designs to maximize energy conversion and minimize system mass. Finally, this Phase I report discusses Mission integration for the case of the Solar Gravity Lens mission vehicle and an Ingenuity follow on mission.

## 1.1 Motivation

We are at a technological precipice of being able to widely visit and study our Solar System and beyond by robotic rovers (e.g. moons, Mars), aerial drones (e.g. Mars Ingenuity), orbiting/flyby probes (e.g. Enceladus Life Finder, JPL Marco) and missions into deep space (e.g. Solar Gravity Lens). The NIAC program under STMD is one of the propelling forces for applying

technological ingenuity in support of these sought after missions. All of these missions require power, and many destinations cannot efficiently use photovoltaic technology.<sup>3</sup> A non-photovoltaic power and energy architecture that is modular, scalable, compact, low mass, long lived and robust to the space environment would enable a host of new missions and vehicle designs.

NASA is investing in several nanosatellite technologies which could be the basis for a modularized, self-assembled in-space architectures and small ground based rovers. NASA is also investing in solar sail propulsion technology (e.g. Solar Cruiser) to explore the possibility of very fast transits through our solar system and beyond (0201 NIAC Phase II). Finally, they are also exploring the next generation in space telescopes (e.g. LUVOIR). Among these and many other missions, an APPLE power system could enable nanosatellites to produce more data (e.g. MarCO), stay on mission longer, to permit high velocity transit space probes that would provide a wider area of space exploration, and better facilitate the flagship missions and to enable very large in space structures to operate in a distributed power mode and thereby reducing harness mass.

## 1.2. RTG Requirements

Radioisotope thermoelectric generator (RTG) technology has been NASA's reliable long-life, non-photovoltaic power system, but these systems have been massive (10's of kg), monolithic, and cannot be accommodated on the small, lightweight space platforms needed for next generation missions to distant destinations. The masses and BOL powers for commonly used RTGs: a) SNAP-9A (12.3 kg, 26.8 W<sub>e</sub>), b) SNAP-19A (13.6 kg, 40.3 W<sub>e</sub>), c) eMMRTG (40.3 kg, 125 W<sub>e</sub>), and GPHS-RTG (57 kg, 300W<sub>e</sub>).<sup>4</sup> In addition, RTGs provide continuous, but declining, power and must either be scaled to accommodate the peak power requirements of a mission (e.g. long distance COMM, imaging, radiometry, etc.) or have onboard energy storage capabilities. Table 1 shows a comparison between APPLE and other applicable deep space power systems for the example of the Juno mission. When the Juno mission was developed, a 450 W (at Jupiter) solar array power system was chosen despite the low solar irradiance at the destination. This array was paired with a 3 kWh battery for peak power operations and power smoothing. Replacing this solar array with a conventional RTG system based on the MMRTG with a 3 kWh battery would result in a system mass of about 160 kg, a 58% reduction in mass over the solar array option. However, with the APPLE design, a much smaller array of double sided APPLE tiles could have been used, resulting in over a 90% reduction in bus mass compared to the solar array + battery Juno design. In addition, since about 150 Wh of electrical power from the Juno solar array were used for systems heating, a covering of single sided APPLE tiles on the vehicle would use the isotope waste heat of the APPLE tile to keep the vehicle warm, and allow a lower power design for a 33% reduction in isotope mass.

Table 1. First order comparison of various power systems sized for the Jupiter JUNO mission.

	Area (m <sup>2</sup> )	Power (W)	Capacity (Wh)	Mass (kg)	Specific Power (g/W)	Specific Energy (g/Wh)
<i>Juno (Solar array + battery)</i>	60	450	3000	380	845	126
<i>MMRTG + battery</i>	NA	450	3000	160	355	53
<i>APPLE, Double Sided</i>	2.25	450	3000	36	80	12
<i>APPLE, Single Sided</i>	NA	300	3000	28	93	9

RTG design efficiency is dependent not only on the ZT of the thermoelectric materials, but also the  $\Delta T$  between the hot and cold shoes. This equilibrium temperature is primarily dependent on the amount of heat generated and the radiator size and efficiency. Existing RTG designs have had to compromise on radiator size, as the relatively compact form factor (cylindrical) meant that the radiator fins had impaired view of space, and extending them would result in additional mass penalties. Using the flat APPLE form factor, radiators with easy access to space for radiation improves radiator efficiency. In addition, if the radiator surface was made to be multifunctional, as an energy storage system, the additional mass of a larger, even more capable radiator would not necessarily accrue the same mass penalty. This can result in a greater  $\Delta T$  for a given isotope mass, and a higher conversion efficiency and lower isotope mass, a critical need given the restricted isotope supply and the safety issues associated with isotope carrying launches.

### 1.3. Current Battery Capability

The state of the art high energy density battery technology for spacecraft are lithium ion cells (Li-ion). With energy densities up to 300 Wh/kg,<sup>5</sup> these cells store the most energy for the lowest mass and volume, displacing older rechargeable chemistries such as NiCd and nickel hydrogen (NiH<sub>2</sub>) cells used in older NASA missions.<sup>6</sup> The challenges of using lithium ion battery technology for spacecraft energy storage in large spacecraft revolves around the thermal control and maintenance of the battery as well the battery wear and ageing. Li-ion cells were designed for terrestrial applications, and as such have an optimal temperature operating range of  $20 \pm 10^\circ\text{C}$ . Battery performance outside these ranges degrades the battery performance and life, and can lead to catastrophic failures.<sup>7</sup> Because of this, the batteries in deep space missions must be kept within this range over mission life through the use of electric heaters which drawn upon the vehicle bus. For large vehicle power systems, the battery is typically placed inside the vehicle, close to the center of mass, as the battery is often one of the heaviest components of the vehicle. This placement interior to the spacecraft does benefit thermal regulation, keeping it with other components such as payloads that need thermal regulation. This interior position also benefits the battery by isolating it from external hazards, namely ionizing radiation and (small) impacts.

For a design that is compatible with small spacecraft, in the 1-20 kg range, there is less deep interior in the vehicle. In addition, for thin, modular spacecraft, the Li-ion battery can no longer be bulky rolls of material in heavy metal cases. In a small, thin, lightweight modular design, the battery must be much thinner, without the benefit of thick steel cell cases and battery boxes. This means the battery is no longer shielded from the radiation and particulate environment of space. Studies conducted at the Jet Propulsion Laboratory and at the Aerospace Corporation showed the effects of radiation on conventional Li-ion batteries. Panasonic B 18650 cells were exposed to 18 Mrad of <sup>60</sup>Co gamma radiation to simulate the effects of radiation sterilization of the battery for planetary protection needs and Jupiter radiation belt ionizing radiation effects. These conventional Li-ion cells showed only minimal initial effects to battery capacity from this irradiation. However, upon cycling the cells showed significant reduction in cycle life, and inspection of the batteries at Aerospace post cycling failure showed extensive damage to the battery materials, as shown in Figure 2. The cells on cycling showed catastrophic failures around 600 cycles, with various hard and soft short circuits causing cell failures. The degradation of the cell materials upon inspection correlated with these failures, as the polymer separator was found to be embrittled and prone to failure, and the anode showing signs of lithium



Figure 2. Li-ion battery electrode materials after 18Mrad gamma radiation exposure and 600 operational cycles. A) shows the embrittled polymer separator adhered to the cathode, and B) shows the discoloration of the anode material, with gold regions that could not discharge.

plating. Both of these failure modes are consistent with degradation of the organic components of the battery, with the polymer separator becoming fragile, and the organic electrolyte polymerizing, resulting in a higher cell impedance linked to dangerous lithium plating. In this test, the cells had a 1mm thick steel case, as well as, for most of the electrode materials, layers of additional shielding battery material due to the jelly roll structure. For planar cell designs to fit in the modular APPLE design, there will be no effective shielding of the battery from external radiation sources, and the battery materials must be robust to ionizing radiation over long mission life.

To remove organic components in an APPLE battery, the existing electrolyte and polymer separators must be replaced with more robust materials. The electric vehicle and personal electronics industries are developing solid state ceramic combination separator/electrolyte systems that should be more resistant to ionizing radiation. There are several systems being developed, including the oxynitride ( $\text{Li}_x\text{PO}_y\text{N}_z$ , LiPON) system, garnets ( $\text{Li}_7\text{La}_3\text{Zr}_2\text{O}_{12}$ , LLZO), phosphates ( $\text{Li}_{1+x}\text{Al}_x\text{Ti}_{2-x}(\text{PO}_4)_3$ , LATP and  $\text{Li}_{1+x}\text{Al}_x\text{Ge}_{2-x}(\text{PO}_4)_3$  LAGP), perovskites, ( $\text{Li}_{3x}\text{La}_{2/3-x}\text{TiO}_3$ , LLTO), germania ( $\text{Li}_{14}\text{Zn}(\text{GeO}_4)_4$ ), nitride ( $\text{Li}_3\text{N}$ ), and sulfide ( $\gamma\text{-Li}_3\text{PS}_4$ ) systems. The radiation hardness of each of these materials has not been determined, but it is likely that the structural and ionic conductivity parameters are more robust to ionizing radiation than organics and polymers due to higher bond strengths and extended crystal structures of these materials. *A radiation hard battery based on the LiPON system is part of the ongoing collaboration between the Aerospace Corporation's Intelligent Battery Group and Oak Ridge National Labs and will be used as the energy storage for APPLE.*

However, these solid state materials typically have a significant drawback in application in comparison to organic electrolytes, as ceramic ionic conductivities are significantly worse. This limits the maximum discharge and charge rates for the batteries, a key limitation for mission application where peak power will be needed for applications like comm, and payloads, and rover motors. The room temperature conductivities for the solid state electrolytes are  $\sim 1 \times 10^{-6} \text{ S cm}^{-1}$  for LiPON,<sup>8</sup>  $1 \times 10^{-4} \text{ S cm}^{-1}$  for LAGP,<sup>9</sup>  $1.0 \times 10^{-5} \text{ S cm}^{-1}$  for garnets,<sup>10</sup>  $1 \times 10^{-5} \text{ S cm}^{-1}$  for



perovskites,<sup>11</sup>  $1 \times 10^{-5} \text{ S cm}^{-1}$  for germania,<sup>12</sup> and  $1 \times 10^{-3} \text{ S cm}^{-1}$  for sulfides.<sup>13</sup> The conductivity for typical commercial Li-ion organic electrolyte systems is  $\sim 1 \times 10^{-2} \text{ S cm}^{-1}$ .<sup>14</sup> These solid state ceramic systems, however, show much better conductivities above  $\sim 60^\circ\text{C}$ ,<sup>15,16</sup> meeting or exceeding typical organic systems, at a temperature which rapidly degrade organic electrolytes. Operating APPLE above  $60^\circ\text{C}$  will avoid the key issue to using solid state batteries for terrestrial applications which typically cannot operate at these temperatures.

In addition, these solid state battery systems are more puncture resistant than the organic systems with polymer separators, as solid materials typically prevent the microshorts that occur during puncture in conventional systems.<sup>17</sup> This puncture resistance is critical for a battery that can face repeated small particle impacts during a mission on a small or thin vehicle that would not be a significant risk in large vehicles. Whereas conventional liquid electrolyte cells could go into thermal runaway upon puncture, a solid state design would not, and perhaps even still be able to function, but even if not, would not damage more of the battery in its distributed, modular shape.

## **1.4. Technology Needs**

In summary, the key needs for a new RTG system that APPLE seeks to meet are a lightweight, modular system to enable a range of vehicle sizes, from microsats and small rovers up to large flagship missions. In addition, to accommodate a wide range of vehicle morphologies and to enhance the RTG efficiency, APPLE has a flat design. This shape allows for additional radiator surface for efficient radiation and a higher heat-to-electricity conversion. This flat, lightweight design requires the active battery materials to be hardened to radiation exposure to prevent battery performance decline over life. As seen in the mission technology and design section below, APPLE will enable a new class of deep space missions built around a robust, flexible, multifunction power architecture.

## 2. Radiation Simulations

Throughout Phase I of this project, radiation simulation efforts evolved to meet dynamic needs of the project as the design evolved. The APPLE design uses a flat unit for spacecraft design flexibility for thermal regulation. However, this type of design can increase susceptibility to radiation exposure both from the radioisotope source as well as the native space environment, as there was more cross section to intersect external particles, and less shielding mass to prevent isotope particles from impacting sensitive components. It was imperative that we perform radiation simulations for both the isotope and space environments, with the high fidelity geometry possible to estimate radiation dose to the battery layers over the course of a planned mission.

Results indicate that dose due to the space environment drives battery exposure over radiation from the isotope source. Dose in interplanetary space due to solar particle events (SPEs) is dynamic and can be unpredictable. For this reason, we simulated worst-case scenarios to maximize the probability of mission success of the selected design. These scenarios covered high flux solar events in the inner solar system portion of the mission. Dose in interplanetary space due to galactic cosmic rays (GCRs) was found to be concerning due to the high energy of these particles and their associated penetration depth. GCRs can also initiate a shower of secondary particles upon incidence with a material, causing downstream effects. Strategic decisions on launch dates (during solar minimum activity) and mission duration (shortest possible) are thus at least partially driven by space radiation dose concerns.

### 2.1. Radioisotope Selection

The radioisotope sources considered for this design were Plutonium ( $^{238}\text{Pu}$ ), Americium ( $^{241}\text{Am}$ ), and Strontium ( $^{90}\text{Sr}$ ).  $^{238}\text{Pu}$  has a long history of space use with NASA.<sup>18</sup> Despite some concerns with supply,<sup>19</sup> the existing use of this isotope should be streamlined compared to a new isotope source selection.  $^{238}\text{Pu}$  has historically been the isotope of choice for RTGs used by NASA missions, used in their previous RTG designs such as Voyagers 1 and 2, Vikings 1 and 2, Cassini, New Horizons, and the MSL. The isotope has an 87.7 year half-life, and generates 0.57 W/g for pure  $^{238}\text{Pu}$  and 0.502 W/g in its  $\text{PuO}_2$  form, the stable oxide of choice for use. Alternative isotopes with high thermal output and sufficiently long half-life for deep space missions considered in this project were  $^{90}\text{Sr}$  and  $^{241}\text{Am}$ .  $^{90}\text{Sr}$  is typically used in its titanate form for chemical stability, while  $^{241}\text{Am}$  is used as the Am(III) form in  $\text{Am}_2\text{O}_3$ .  $^{90}\text{Sr}$  is an attractive isotope due to its relative abundance from nuclear reactor waste, and  $^{241}\text{Am}$  is the isotope being considered for ESA's RTG designs.<sup>20</sup>

Table 2. Figures of merit for the three RTG isotopes under consideration.

Isotope	Material	Thermal output (metal, W/g)	Thermal output (material, BOL, W/g)	Thermal output (material, EOL-15y, W/g)	Mass (material, g/cm <sup>3</sup> )	Thermal output (material, W/cm <sup>3</sup> )
$^{238}\text{Pu}$	$\text{PuO}_2$	0.57	0.50	0.45	11.5	5.77
$^{90}\text{Sr}$	$\text{SrTiO}_3$	0.95	0.46	0.32	5.11	1.31
$^{241}\text{Am}$	$\text{Am}_2\text{O}_3$	0.11	0.10	0.10	11.77	1.21

However, these isotopes decay through widely different mechanisms, and release their energy via different particle emissions. These particles must be captured through interaction with the RTG mass to generate heat. The decay products of each of these three sources vary in both species and energy, with  $^{238}\text{Pu}$  emitting 5.593 MeV alpha particles,  $^{241}\text{Am}$  emitting 5.478 MeV alpha particles and 59 keV gamma rays, and  $^{90}\text{Sr}$  emitting 0.546 MeV beta particles (electrons). Figure 3 shows the average penetration depths of the isotope decay particles in common RTG and spacecraft materials.<sup>21,22,23</sup> These values were calculated using National Institute of Standards and Technology (NIST) lookup tables of stopping power, range, and/or mass attenuation coefficients for specific decay products and target materials. The  $^{238}\text{Pu}$  alpha particles have very large interaction cross sections, meaning that they have very short penetration depths for energy capture. Typically, this energy is captured within the  $^{238}\text{Pu}$  oxide material itself, with the remaining captured in the isotope cladding.  $^{90}\text{Sr}$ , on the other hand, releases its energy in highly penetrating beta particles, requiring substantial amounts of material to capture the released energy. RTGs based in  $^{90}\text{Sr}$  typically use large amounts of dense material to fully convert the radiation to heat, increasing their mass, and would have a negative impact on APPLE energy density.  $^{241}\text{Am}$  is similar in some ways to  $^{238}\text{Pu}$ , as it releases its energy in alpha particles, but also releases 59 keV gamma rays, which penetrate much farther than alpha particles, if not so far as the  $^{90}\text{Sr}$  beta particles. While  $^{238}\text{Pu}$  can capture most of the energy within the Pt clad isotope core,  $^{90}\text{Sr}$  would need 2-3x as much Pt to efficiently capture its beta particles compared to capturing  $^{241}\text{Am}$ 's gamma rays, which needs about 200  $\mu\text{m}$  of Pt. This does not account for human shielding requirements for the beta and gamma rays, only the thermal conversion needs of an APPLE system.

In addition,  $^{238}\text{Pu}$  has higher volumetric and gravimetric energy densities compared to either  $^{90}\text{Sr}$  or  $^{241}\text{Am}$ , especially at end of life, as shown in Table 2. Therefore,  $^{238}\text{Pu}$  was selected as the primary radioisotope source for this design moving forward, but  $^{90}\text{Sr}$  and  $^{241}\text{Am}$  were considered as well, though the isotope radiation capture mass (Pt cladding) would be increased.

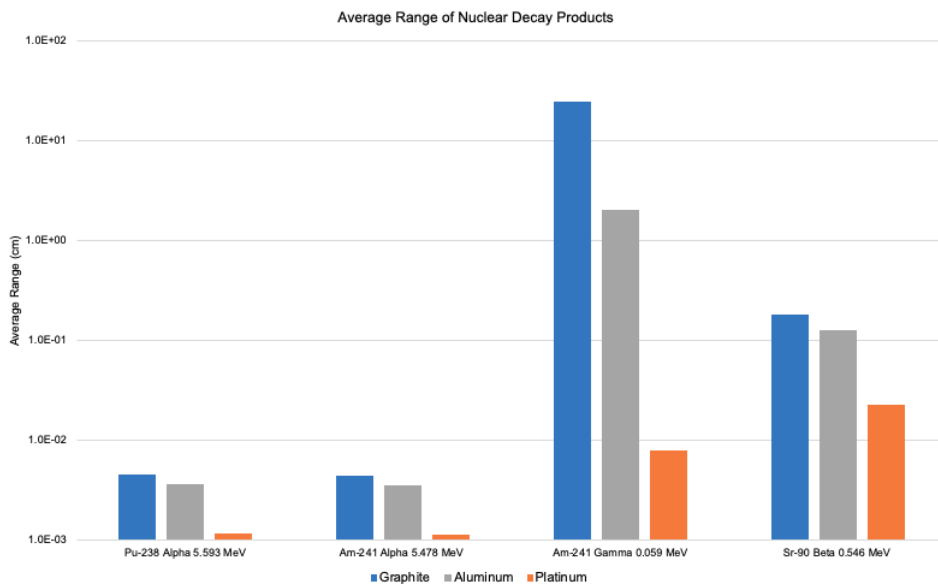


Figure 3. Average penetration depths of decay particles from  $^{238}\text{Pu}$ ,  $^{90}\text{Sr}$ , and  $^{241}\text{Am}$  in common materials. The long capture length for  $^{90}\text{Sr}$  betas impacts its use in lightweight RTGs.

## 2.2. Methodology and Results

Radiation models and simulations for this project were developed within the GEANT4 simulation toolkit.<sup>24,25</sup> GEANT4 is well-validated for modeling space hardware and both nuclear and space radiation environments.

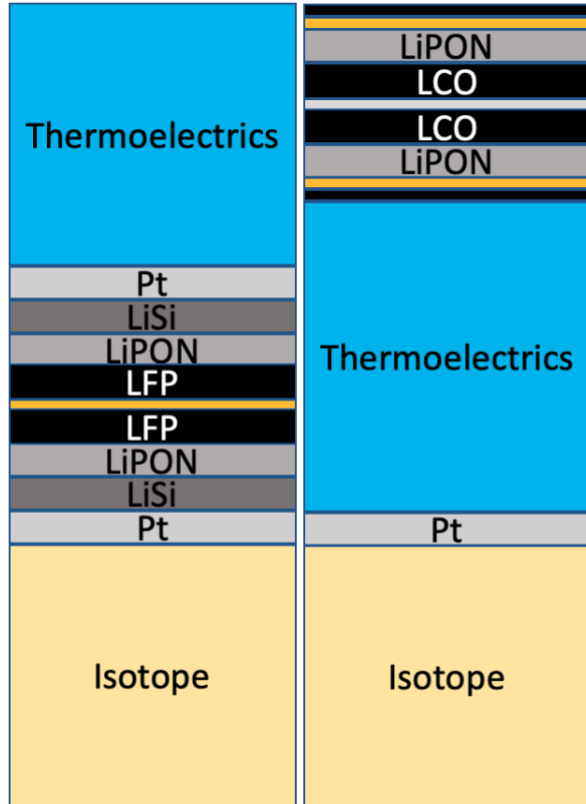


Figure 4. An example of battery and thermoelectric layer geometries. On the left, the battery on isotope design, and on the right, the battery on radiator design.

We initially simulated the geometry of the battery layers as shown in Figure 4 on the left. Throughout the project, this geometry continued to be modified as the design evolved. Materials for each layer were modeled as a percentage mixture of the atomic makeup of each molecule. This first design simulated SiGe thermoelectrics, used previously in the GPHS-RTG, and the battery design and placement was based on the initial APPLE design, that used a battery on isotope design. This design was intended to use the radiation hard battery as a radiation shield for other components of the APPLE tile and spacecraft. This initial battery design was a high temperature battery that used lithium silicide as the anode and lithium iron phosphate as the cathode material; both materials being stable at the high temperatures of the isotope. Later simulations used the lithium metal-LCO battery in a battery on radiator design.

We modeled the nuclear radiation environment for each of the three radioisotope sources ( $^{238}\text{Pu}$ ,  $^{241}\text{Am}$ ,  $^{90}\text{Sr}$ ) as planar sources in GEANT4 and propagated decay products in the direction of the battery layers. As displayed in Figure 5, the

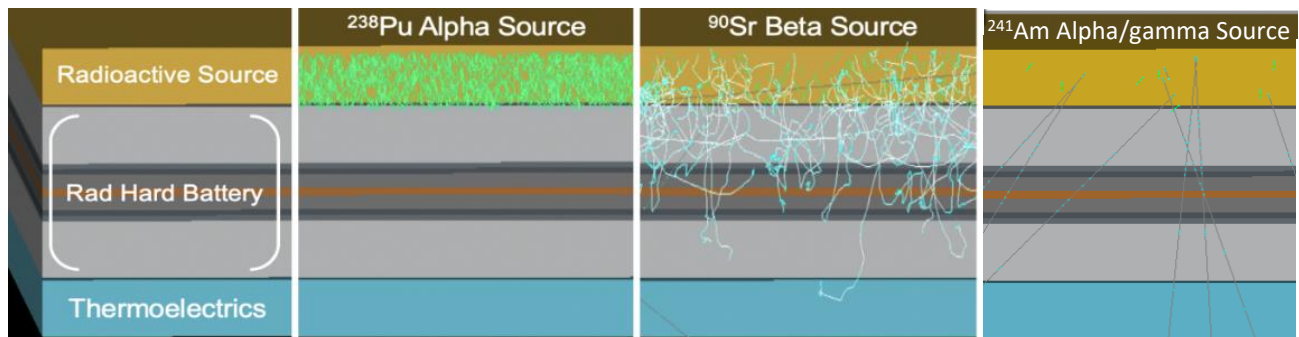


Figure 5. Geant4 simulation of radioisotope source and battery layers, showing particle tracks and interaction points of primary alpha, beta, and gamma radiation. The green tracks are alpha particles, the teal tracks are beta particles, and the gray tracks are gamma rays.

alpha particles from  $^{238}\text{Pu}$  and  $^{241}\text{Am}$  penetrated a very short distance and were absorbed in the immediately neighboring layer of material, beta particles from  $^{90}\text{Sr}$  and gamma rays from  $^{241}\text{Am}$  penetrated further and were absorbed in deeper layers of the battery, though some of the radiation penetrated through the entire stack continued on into space, especially for sims with thinner isotope cladding.

It was determined from these simulations that the initial concept of using the radiation hard battery as a radiation shield, preventing ionizing radiation from the isotope from reaching other parts of APPLE and the vehicle was unnecessary. The battery itself was relatively thin and not composed of materials that excelled at intercepting ionizing radiation. In addition, for the alpha sources no radiation was escaping the isotope material or its refractory metal cladding. For more penetrating particles like gammas and betas, the battery had little or no effect on radiation exposure. Further, it was decided that locating the battery at the hot shoe interface substantially restricted battery and thermoelectric performance by restricting the temperature of the interface (reducing TEM conversion efficiency) and restricting the battery materials (lowering battery energy density) (see Thermal Design and Battery Materials sections below). It was decided at this point to convert the design to a battery on radiator design over the battery on isotope design in the first APPLE design.

### 2.3. Solar and Galactic Radiation Exposure

Regardless of the battery location, either on the isotope or on the radiator, the isotope radiation was not the only ionizing radiation risks. Due to the thin profile and lightweight materials used in the APPLE design, external radiation sources are also an important source of potential damage.

We modeled the interplanetary space radiation environment for both solar particle event (SPE) and galactic cosmic ray (GCR) radiation. The space environment model was based on NASA's Badhwar-O'Neill 2014 model for GCRs,<sup>26</sup> the August 1972 SPE spectra as a "worst-case" example, and typical "average" SPE spectra and frequency based on solar cycle data.<sup>27,28</sup> Separate simulations were run to calculate dose equivalent from an average SPE, worst-case SPE, and daily GCRs. The effect of the 11-year solar cycle on the frequency and intensity of SPEs was also considered, and the worst-case dose estimates were selected for each case. These

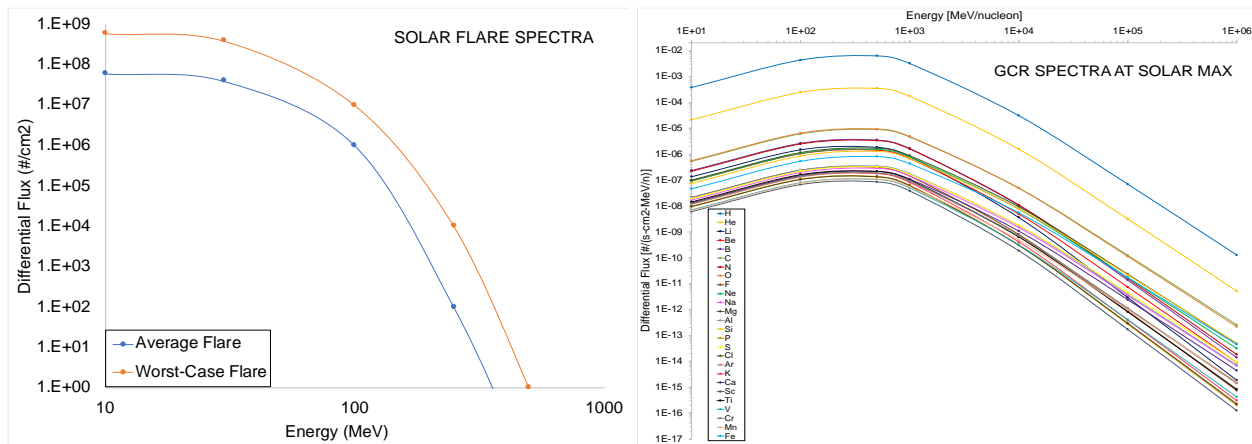


Figure 6. Simulated SPE (left) and GCR (right) spectra.

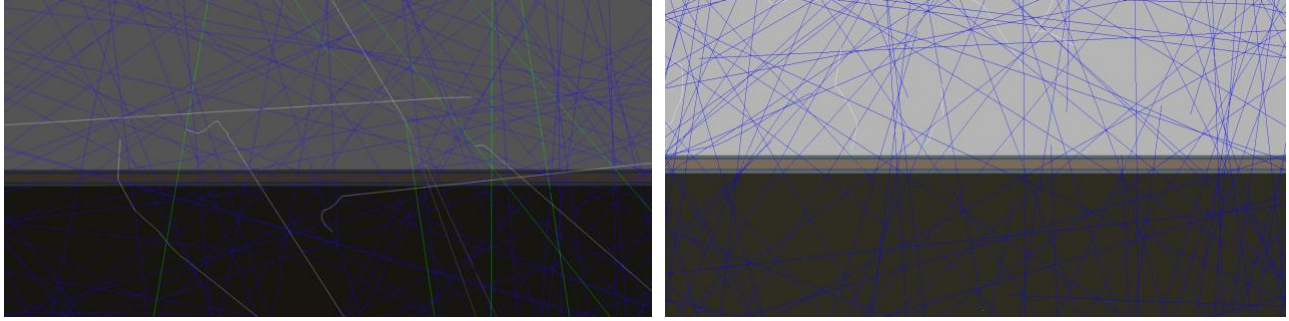


Figure 7. Space radiation incident on the battery stack; (left) GCR, (right) SPE. The battery is the thin layers in the middle, between the aerogel (top) and a radiator (bottom).

sources were modeled in GEANT4 as large spherical sources with particles incident across a wide range of angles to simulate the space environment. The particle and energy spectra of the sources were simulated as shown in Figure 6.

As displayed in Figure 7, SPE protons and GCR protons, alphas, and heavy ions easily penetrate the entire battery stack, depositing energy (dose) throughout the volume of each layer. Shielding these high energy particles is difficult, requiring a large mass of passive shielding materials. Utilization of radiation hard materials for the battery will be needed to prevent this radiation from degrading battery performance, but not all vehicle components can be so hardened. Therefore, clever management of exposure of sensitive components of the vehicle to the space radiation environment is typically the most cost- and mass- efficient strategy. This likely entails careful selection of mission launch date and duration to minimize exposure to the solar cycle. Our team recommends launch of interplanetary missions during the solar minimum period of the 11-year solar cycle to reduce the risk of large doses from intense, more frequent solar flares during solar maximum while in the inner solar system. If launch is to be at solar cycle maximum, a thicker shielding material could be added to the APPLE design, in addition to more shielding for the rest of the vehicle.

## 2.4. Calculated Battery Radiation Dose

For the battery radiation testing portion of this project, the radiation dose from expected sources was calculated. Absorbed dose ( $D$ ) is the fundamental dose quantity that describes the energy deposited by ionizing radiation. It has the SI unit of joule per kilogram (J/kg) or gray (Gy) and is given by:<sup>29</sup>

Equation 1. 
$$D = \frac{d\bar{\epsilon}}{dm}$$

where:

$d\bar{\epsilon}$  = mean energy imparted by ionizing radiation

$dm$  = mass

Absorbed dose was calculated in our simulations by collecting the energy deposited in the scoring volume (water phantom) per unit mass. This calculation was done within the GEANT4



code and also includes a calculation of the standard error of the mean dose deposited in the volume of interest. This data for SPE dose was calculated for 1 AU, and will decrease as  $1/r^2$  for distance from the sun. Once in the outer solar system (past Mars) vehicle dose will primarily be from GCR, unless a worst case SPE occurs.

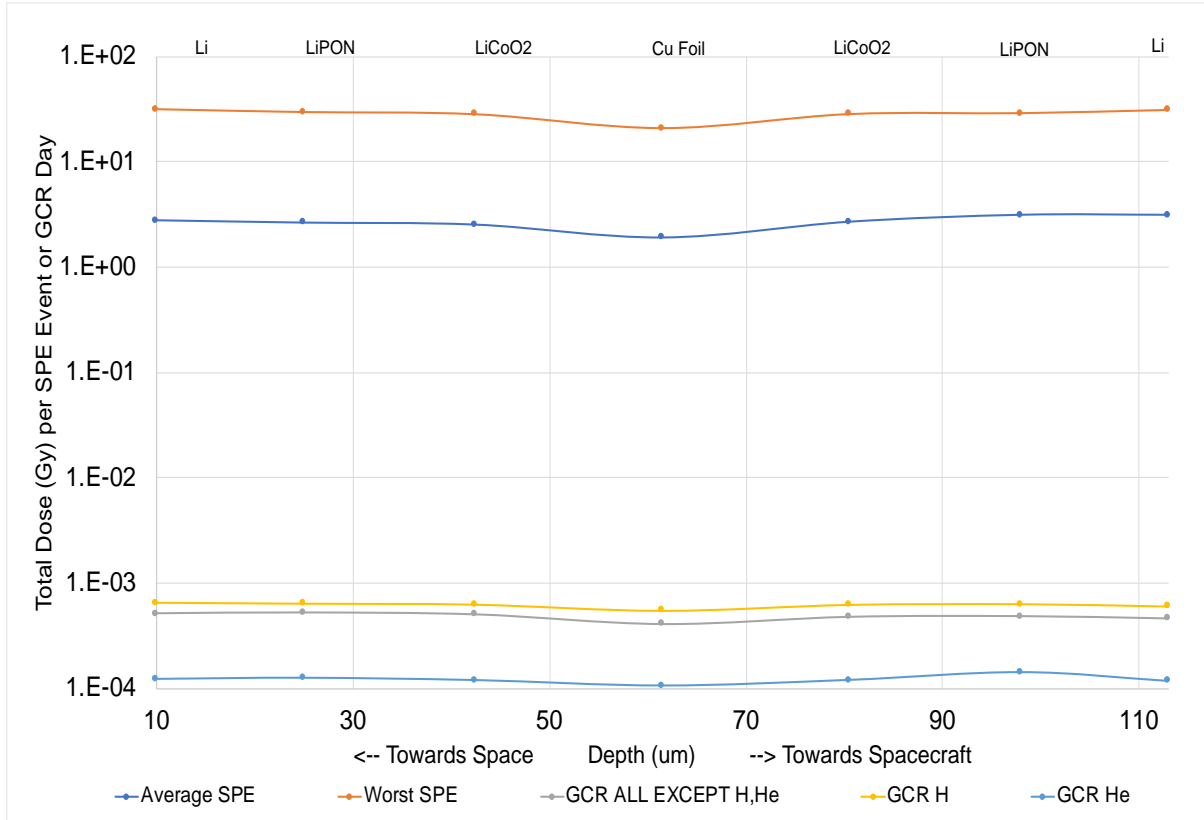


Figure 8. Total dose per SPE event or GCR "day" in interplanetary space for the battery.

Dose to the battery materials per solar particle event (SPE) or galactic cosmic ray (GCR) "day" in interplanetary space is displayed in Figure 8. The data in this plot shows dose deposited in each layer from an "average" SPE, "worst-case" SPE, GCR protons (H), GCR alphas (He), and the remainder of GCR heavy ions ( $Z=3$  to  $Z=26$ ). From this figure, we conclude that the dose due to "average" SPEs, "worst-case" SPEs, and GCRs are fairly constant throughout the battery layers. This agrees with what we expect from high energy, high atomic number (HZE) particles that are extremely penetrating and require a large mass of passive material to shield against. Space radiation dose deposited to the battery was found to be significant in these simulations. Results show GCR dose to the battery for a direct transit 2-year flyby mission to Jupiter to be on the order of 0.5 Gy with additional SPE dose on the order of 5 Gy to 40 Gy depending on the solar cycle position and the occurrence of a "worst-case" SPE. For indirect transit missions, which spend more time in the inner solar system for gravity assists to permit orbital injection, dose will be heavily dependent on the solar events during the mission and would have to be calculated accordingly.

Figure 9 shows the calculated deposited dose in the battery for a direct transit mission to an outer solar system destination. While in the inner solar system, dose accumulation is almost entirely from solar flare events. This simulation uses the average SPE dose calculated, not the worst case SPE dose. Approximately past Jupiter's distance, dose accumulation from GCR dominates. After passing this distance, for any mission destination GCR will be the dominant source of radiation. This does not account for any additional radiation present at the destination, such as the high energy electrons and protons in Jovian radiation belts.<sup>30</sup>

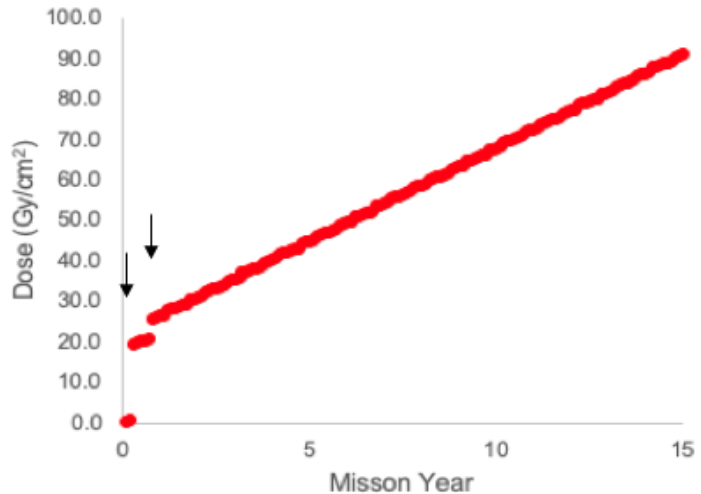


Figure 9. The total dose from GCR and average solar flares on a direct transit mission to beyond Jupiter. The arrows indicate the strong influence of solar flares on the accumulated dose while in the inner solar system.

## 2.5. Translation of Dose Equivalent to Dose

Doses calculated in simulation can then be compared to the doses deposited during laboratory radiation testing to begin estimating and calibrating the ratio of dose to battery material damage. A concern in comparing calculated simulation dose to measured laboratory dose is a consideration of units. Our simulations report absorbed dose in the SI unit of Gy. This unit converts to the conventional unit of rad by a factor of 100. However, the laboratory measurements used in this work use dose equivalent, which is in the conventional unit of rem. Rem is a unit of exposure, not dose, and is designed as an equivalent dose for a human. The testing facility used for this experiment was designed for human exposure rather than to simulate space exposure. This rem unit can be converted to the dose equivalent SI unit of Sv by a factor of 100, but the conversion between absorbed dose and dose equivalent still remains.

Absorbed dose is scaled to dose equivalent via one of several methods including the radiation quality factor (Q), relative biological effectiveness (RBE), or radiation weighting factor ( $w_R$ ) to account for the relative biological effect of different types and energies of ionizing radiation (ICRP 2007). For the purposes of this project, the laboratory sources have low RBE (~1) and thus the margin of error between converting absorbed dose and dose equivalent is very small. For this specific case, we can compare the absorbed dose from simulation (Gy) to the dose equivalent measured in the laboratory (rem converted to Sv) without significant concern for conversion error.

## 2.6. Mission Applications

The above simulations and calculations apply to an APPLE mission solely to interplanetary space where the space radiation environment has been characterized by prior sensors and spacecraft. If APPLE is to be dispatched on a mission to a new or poorly characterized environment, new models, estimates, and simulations will be required. For example, if an



APPLE mission were to spend significant portion of its mission in the near vicinity of the Sun, another planet, moon, or asteroid, additional considerations regarding trapped radiation (similar to Earth's Van Allen belts), X- or gamma ray radiation, albedo (reflected) radiation from the surface, etc. must be considered and accounted for.

In the example of a direct transit 2-year Jovian mission, APPLE would spend the majority of its time in interplanetary space, which we have simulated and studied as part of this project. During the portion of the mission in the Jovian environment, however, additional trapped electron radiation will likely be present. Additionally, a portion of the SPE and GCR radiation will be blocked by the planet itself, so additional simulations will be needed based on the specific geometry and location of the vehicle to determine the effects to total dose in the Jovian environment. This would apply to any mission destination that has significant radiation source, and should be simulated for each mission path.

## **2.7. Next Steps in Phase II**

Proposed follow on work for this segment of the project include improved fidelity of the radiation simulations. Specifically, we plan to update the geometry as the overall design advances with increased knowledge of the battery structure and thermal environment. We also plan to conduct further scenario-based simulations for a variety of potential mission types, such as radiation simulations of the high energy radiation belts around Jupiter. This will allow the team to focus laboratory radiation exposures on the most feasible mission concepts.

### **3. Battery Design and Testing**

#### **3.1. Need for a Solid State, Radiation Hard Battery**

A radiation hard, solid state battery is needed for the APPLE design due to both the potential incident radiation from the isotope source as well as from external radiation sources such as solar particles and galactic cosmic radiation, as noted above. Due to the long duration of the missions planned for using APPLE, 15-50 years, the expected dose of radiation to the battery can be high. As seen in destructive physical analysis of conventional Li-ion batteries (Figure 2), the organic components of conventional cells degrade under ionizing radiation, even when in a steel case where the jelly roll design results in substantial self-shielding. With the proposed flat design of the battery in APPLE, the lack of a solid metal case for the cell components, and the necessary placement of APPLE on the exterior of the vehicle the battery materials will be uniquely exposed to radiation during mission. To avoid degradation over life, a solid state, radiation hard battery was proposed. This design would remove the organic electrolyte, typically a carbonate, ether, glyme, or polymer in favor of a solid ceramic material that would not be able to polymerize in response to an ionization event. In addition, this material has a much higher operational temperature range, unlike the organics, which are typically restricted to a narrow ( $20^{\circ}\text{C} \pm 10^{\circ}\text{C}$ ) temperature range. The typically wide temperature operating range of ceramic electrolytes ( $60^{\circ}\text{C}$  to  $200^{\circ}\text{C}$ ) allows for the removal of active battery temperature regulation, and to use passive regulation based on the generated heat from the isotope decay and a radiator. This not only removes a failure prone system, but also reduces the bus power needed to regulate battery temperature from the power requirements, allowing for a smaller power source.

Neutron irradiation is also a concern for the APPLE battery. Plutonium(IV) oxide emits neutrons many more neutrons than  $^{238}\text{Pu}$  metal, at the rate of  $2.1 \times 10^4$  n/sec/g of plutonium-238.<sup>31</sup> This production of neutrons is approximately 10x the neutron flux from  $^{238}\text{Pu}$ , with the remaining flux of neutrons coming from the interaction of the  $^{238}\text{Pu}$  alpha particles interacting with the oxygen atoms of the oxide. This production of neutrons from the isotope source is the reason that  $^7\text{Li}$  was chosen as the lithium isotope for the radiation hard battery, even though natural Li sources are ~93%  $^6\text{Li}$ .<sup>32</sup>  $^6\text{Li}$  has a cross section for neutron capture approximately 29,000x higher than  $^7\text{Li}$ .<sup>33</sup>  $^6\text{Li}$  when undergoing neutron capture produces a triton and an alpha particle, which both destroys the  $^6\text{Li}$  needed for energy storage chemistry, but also generates particles ( $^3\text{H}$ ,  $\text{He}$ )<sup>34</sup> which will form gasses that can nucleate inside the battery forming stress bubbles which can fracture the solid state battery structure and further reduce battery performance. Using  $^7\text{Li}$  was determined to be critical for a battery in any proximity to  $^{238}\text{Pu}$ . The neutron flux from the  $^{238}\text{Pu}$  source will not be significantly shielded before it reaches the battery in either the initial design of APPLE, with the battery at the hot shoe, mounted on the isotope source, or in the final Phase I design of APPLE with the battery at the radiator interface.

#### **3.2. Solid State Radiation Hard Battery Fabrication**

Solid state, radiation hard batteries for this study were fabricated from isotopically enriched materials grown in thin film form based on the well-established LiPON based all solid-state battery developed at the Oak Ridge National Laboratory.<sup>35,36</sup> These cells consist of vapor

deposited cathode films grown on a platinum coated  $\text{Al}_2\text{O}_3$  substrate. The cathode films were annealed at  $700^\circ\text{C}$  in air to compensate for oxygen deficiency and crystallize the materials into the layered  $\text{LiCoO}_2$  (LCO) structure. A 1 mm glassy LiPON solid electrolyte ( $\sim\text{Li}_{3.3}\text{PO}_{3.6}\text{N}_{0.36}$ ) was vapor deposited on the LCO followed by a capacity matched silicon film for the full cell configuration. As discussed above, silicon was chosen for both radiation tolerance and high temperature electrochemistry. This first fabrication of cells was performed for the APPLE design that used a battery on isotope design, and as such had higher temperature requirements for the materials.

Sputtering targets were made using naturally abundant Li sources and  $^7\text{Li}$  enriched materials to generate the cells and their controls. The  $^7\text{LiPON}$  target was prepared by precipitation of  $^7\text{Li}_3\text{PO}_4$  from the reaction of  $^7\text{LiOH}$  and  $\text{H}_3\text{PO}_4$ . Stoichiometric amounts of reagents were added dropwise to deionized water resulting in a precipitation reaction. The solution was heated to dryness and the powders collected and ground to obtain the right grain size and tap density to press a dense sputter target. The material was sintered at  $300^\circ\text{C}$  to form a 2" diameter sputter target which was bonded to a copper plate and used for the film growth. To make the enriched cathode material  $^7\text{LiOH}$  was mixed with stoichiometric amounts of  $\text{CoCO}_3\cdot\text{H}_2\text{O}$  and rolled for 24 hours on a ball mill with enough isopropyl alcohol to wet the slurry. The material was dried on a hot plate and sintered at  $500^\circ\text{C}$  to form LCO precursor. This precursor was pressed into a  $2\frac{1}{2}$ " diameter pellet which was annealed at  $800^\circ\text{C}$  to form a dense sputter target (2" diameter).

Sputter targets were loaded in a vacuum chamber to grow the heterostructures. Figure 10 shows a representative image of the as grown LCO films. In this configuration the active area is about  $1.5\text{ cm}^2$  with a thickness of about 3 mm for the LCO and 1 mm for the LiPON. The metal tabs to the left and right are platinum which provides electrical contacts to the potentiostat for the electrochemical testing. A 150  $\mu\text{m}$  silicon film was deposited on the surface to match the capacity of the LCO.

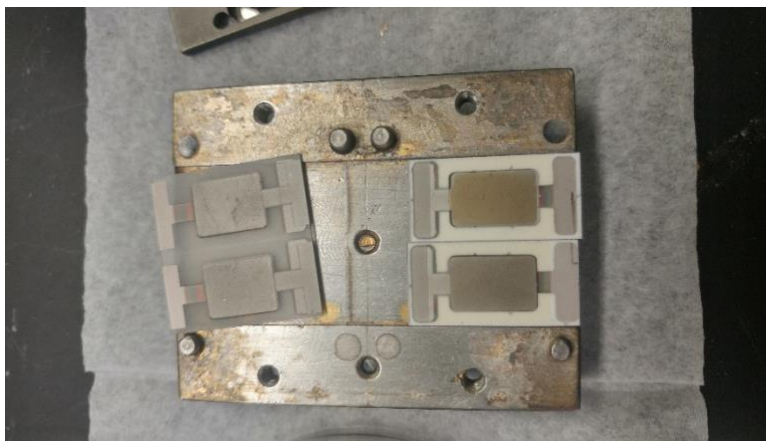


Figure 10. Image of solid-state battery cells built 4 at a time for this testing.

### 3.3. Electrochemical Activation and Testing

A special cycling configuration was assembled to evaluate the electrochemistry and test the radiation tolerance of the batteries. Traditionally, thin film solid state batteries are cycled in argon filled steel cans. For this work we developed a modified pouch cell configuration (Figure 11). The cells from Figure 10 were positioned in the custom formed pouch cell using standard battery pouch cell material (MediaTech Company). Nickel tabs were used to make electrical contact with the platinum current collectors. Contact was made through the vacuum sealing of the pouch which pulled the nickel in contact with the Pt. This configuration resulted in a resistive contact ( $\sim 100$  Ohm) that needs addressed in subsequent work likely due to the thin film platinum and ridged nickel generating limited points of contact. However, the contact was sufficiently robust to allow proof of concept testing of the cell. The specific configuration was selected for the radiation testing portion of the project, and used a case/pouch of as little material as possible to avoid the exterior of the cell to impact the radiation dose, especially since the APPLE design has a limited outer case material. The polymer/Al pouch material used had a low radiation capture cross section compared



Figure 11. Pouch cell configuration where cells from Figure 10 were packaged in battery pouch cell material. Electrical contacts were made with nickel tabs.

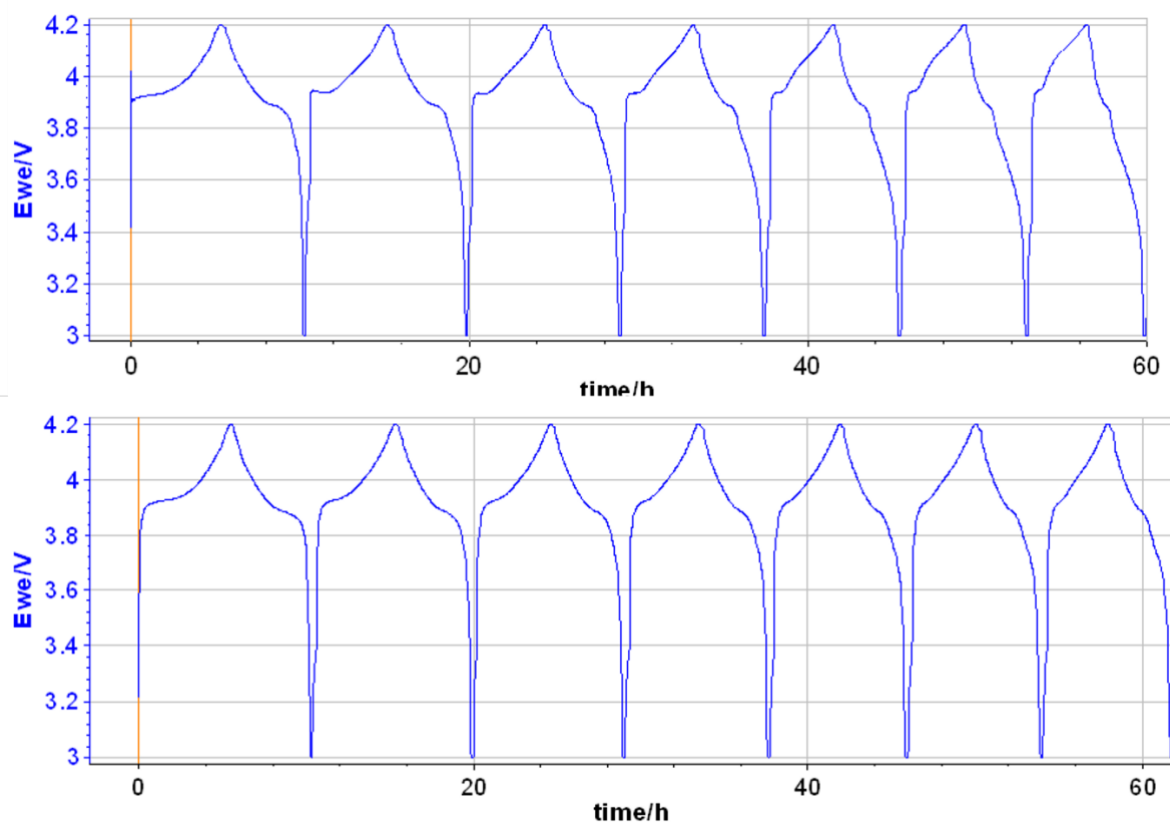


Figure 12. Formation cycles for LCO full cells with natural (top) and  $^7\text{Li}$  enriched targets (bottom).

to typical steel case materials used in conventional Li-ion cells. In addition, the cells could fit into the source drum and be retrieved with little activation from the pouch material. In this type of testing the irradiation generated activation of materials is a major concern, and results in massive disposal costs. This configuration reduced the waste associated with activated steels and trapped any generated tritium from the neutron capture and decay of  ${}^6\text{Li}$  in the naturally abundant battery configurations.

Cells were cycled at a rate of C/6 at room temperatures in the pouch cell configuration for activation and initial characterization. Figure 12 shows representative cycling data for full cells built from naturally abundant and  ${}^7\text{Li}$  enriched materials (top and bottom respectively). The electrochemical data shows an evolving voltage profile. The origin of this is related to the activation of the silicon anode and increases in cell internal resistances from the current collectors, changes in the Si, volume expansion, and evolution of the LCO. The two cell types, natural abundance Li materials and  ${}^7\text{Li}$  materials were substantially similar in cell performance and capacity in these characterization tests. These cell characterizations will be used post irradiation to compare cell performance before and after testing for material breakdown.

### 3.4. Radiation Testing of Cells

After cell electrochemical activation and characterization for radiation testing these cells were loaded into drums containing Americium-Beryllium (AmBe) sources with dose rates of up to  $6.6 \times 10^6$  neutrons/second (17.5 K mrem/hour at 2 cm neutron/ 2.4 M mrem/hour at 2 cm gamma), shown in Figure 13 and Figure 15. Because neutron instruments does not fit inside the shielded drums, we placed neutron dosimeters into the cavity with the batteries. Neutron dosimeters were irradiated for the same time duration as battery irradiation time. In this manner we, rely on the calibration process at ORNL where they have methods/algorithms to extrapolate the dose from AmBe sources. From this passive dosimetry we will estimate the adsorbed dose on the samples which will be used to model the dose imparted on the batteries. We also need to model the detector geometry and the drum inner barrel itself to capture the neutron losses due to scatter and self-absorption within the drum made with borated poly-beads in a plaster cermet. There will also be some neutron gain due to neutron back reflection from elastic and inelastic scatter, which will also affect the neutron energy spectrum due to inelastic and elastic neutron scatter, which will also result in a change in the associated gamma flux due to the inelastic neutron scatter. The batteries were placed around the source in the barrel such that they are oriented relative to the source at a fixed distance. An analysis of the predicted radiation dose is shown in Figure 14, with the total dose from the combined neutrons and 4.438 MeV gammas predicted over the cell areas. Originally cabling was going to be run into the drums to cycle the cells during testing. This was abandoned to avoid activating the copper in the cables and minimize waste costs. Instead, cells were going to be removed after dosing and cycled offline. Testing protocols



Figure 13. Image of radiation source used in this work.

were developed in Phase I but have been hindered by COVID vaccination issues at the facility that should be resolved in late January 2022.

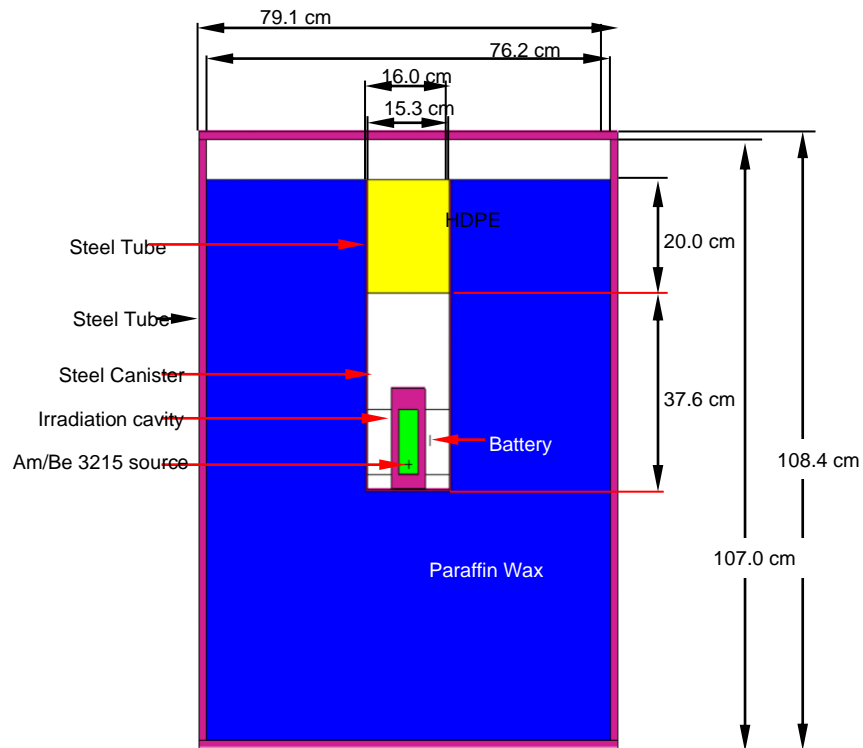


Figure 15. Location of the battery on the AmBe radiation source.

Am-Be-3215:

- Neutrons:  $S_n = 6.81E+06$  n/s
- Associated Am/Be Gamma;  $E = 4.438$  MeV
- $S_\gamma = (0.67 \times S_n) = 4.56E+06$  phot/s

Total Dose Rate due to:  $S_n(n) + S_n(n,g) + S_\gamma$

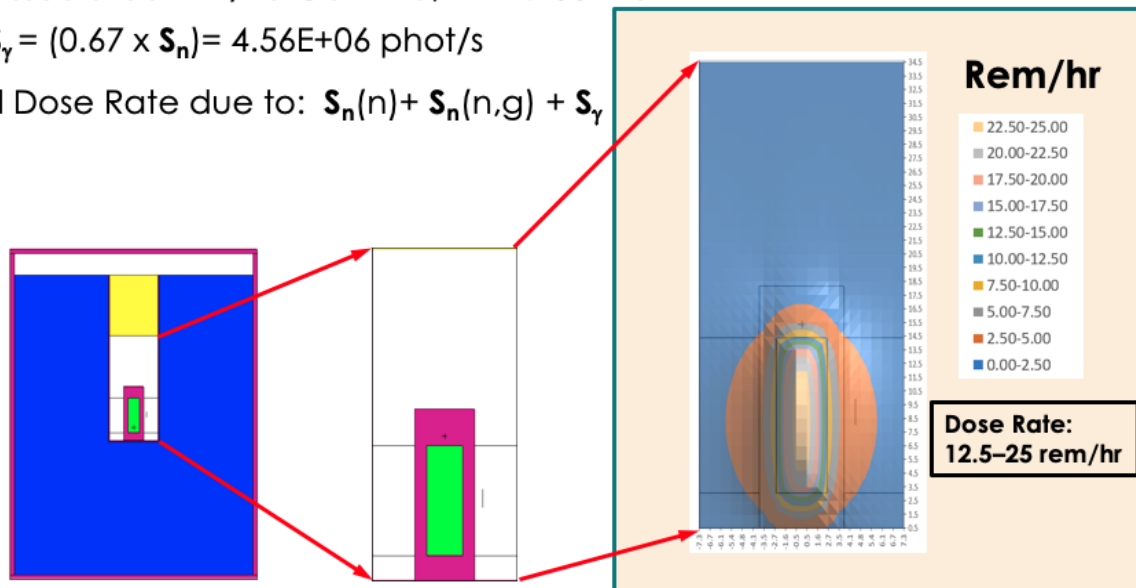


Figure 14. Dose analysis for the cells under test from the AmBe radiation source.

### 3.5. Next Steps in Phase II

In Phase II we will continue to use this platform to build dense batteries but switch to a  $\text{LiMn}_{1.5}\text{Ni}_{0.5}\text{O}_4$  cathode that will be grown to 25-30  $\mu\text{m}$  thicknesses. The team has been developing processes to prepare electrodes at this thickness to increase energy density without sacrificing transport and interfacial stability through controlled nucleation and growth of the cathode films (to be published). This thickness and electrode will be sufficient for radiation testing while providing a 4.6+ V battery system. Further, one eliminates the slow diffusion of cobalt into the solid electrolyte at elevated temperatures by moving to this electrode while imparting structural stability by using the 3D spinel electrode over the 2D  $\text{LiCoO}_2$  while enhancing diffusion pathways. The ultimate goal is a 100  $\mu\text{m}$  thick electrode with a solid electrolyte and lithium anode to provide the power/energy density required and form factor required for the APPLE platform. This will likely be performed using a combination of sputtering, as a seed layer, along with a dense cathode layer prepared by tape casting.

For the Phase II APPLE program thick LMNO electrodes will be vapor deposited and annealed to form dense cathode films. Samples will be grown on thin substrates amenable to TE growth including Ir or Pt. These substrates act as a current collector and substrate to bond the TE layers. Capacity matched silicon electrodes will be prepared through vapor deposition. Note, the cathode will be made from isotopically enriched Li sources ( $^7\text{Li}$ ) to moderate interactions with secondary neutrons resulting in neutron capture and decay into  $^3\text{H}$ ,  $^4\text{He}$ , and high energy gamma radiation, as well as have the potential to include specific isotopes of Ni (e.g.  $^{60}\text{Ni}$ ) which may be important to impart radiation hardness with various sources. Electrodes will be tested in planar geometries using standard electrochemical cycling protocols developed at ORNL. This includes testing at elevated temperatures (50-100°C) and the development of pouch cell configurations for testing in radiation environments. Witness samples will be cycled without radiation exposure to deconvolute materials issues from radiation induced defect issues. Further, samples will be subjected to aging at elevated temperatures and investigated using XPS depth profiling to confirm transition metal stability.

To evaluate the survivability of the electrodes proposed in this work representative cells will be evaluated at the Oak Ridge National Laboratory's Detector Calibration Facility and local fixed radiation drums. The Detector Calibration Facility is expanding its mission to enable testing of materials under extreme environments, with well controlled doses and flux rates. Materials will be evaluated with simulated radiation sources to mimic the expected radiation profile of the potential isotope source. The voltage profile and capacity retentions will be measured periodically (rather than continuously) to evaluate the effect of radiation on the APPLE platform with time (months) and project out to end of mission life. This intermittent cycling protocol will mimic conditions expected for deep space operation where batteries will be cycled x times per month/year consistent with hibernation during transit. The results will be related to processing conditions to prepare the electrodes, cell performance, and capacity fade for witness batteries not exposed to radiation. Batteries will be saved to perform post-mortem analysis in future work. Particularly we are interested in using the batteries as a dosimeter to measure radiation in deep space potentially increasing the utility of the battery beyond just a power source.



## 4. Thermal Design Simulations

### 4.1. Introduction

The APPLE power system concept a small, planar, modular design with an overall minimum thickness, targeting ~1 cm. This enables the utilization of the APPLE system in the widest range of vehicle designs including flat designs, utilization of surfaces such as solar sails or other spacecraft surface. The key constraining factor in the design of APPLE is the thermal gradients within the device, as the core energy generation technology is thermoelectric materials (TEM) to convert heat to electrical energy and dissipate heat to the environment through a combination of radiators to space and heat pipes to the rest of the vehicle. A decaying radioisotope provides the heat source for the TEM, and the radiation hard battery in the initial design acted as a radiation shield to other components. Figure 16 shows the starting APPLE design concept this project iterated from in Phase I. This design placed the radiation hard battery between the isotope heat source and the thermoelectrics and sought to use the battery as a radiation shield for vulnerable components of the device and vehicle. With the target temperatures for the thermoelectrics being ~400°C, this meant that the battery would also need to not only function at this temperature, but also be able to cycle repeatedly through all of its charge states without material breakdown.

This design then uses the battery as a radiation shield and keeps the battery within the temperature range of less than 400°C and above 60°C. This lower temperature range was based on current minimum capabilities of solid state electrolytes for batteries based on the ionic conductance of the materials. As discussed above in the Current Battery Capability section,

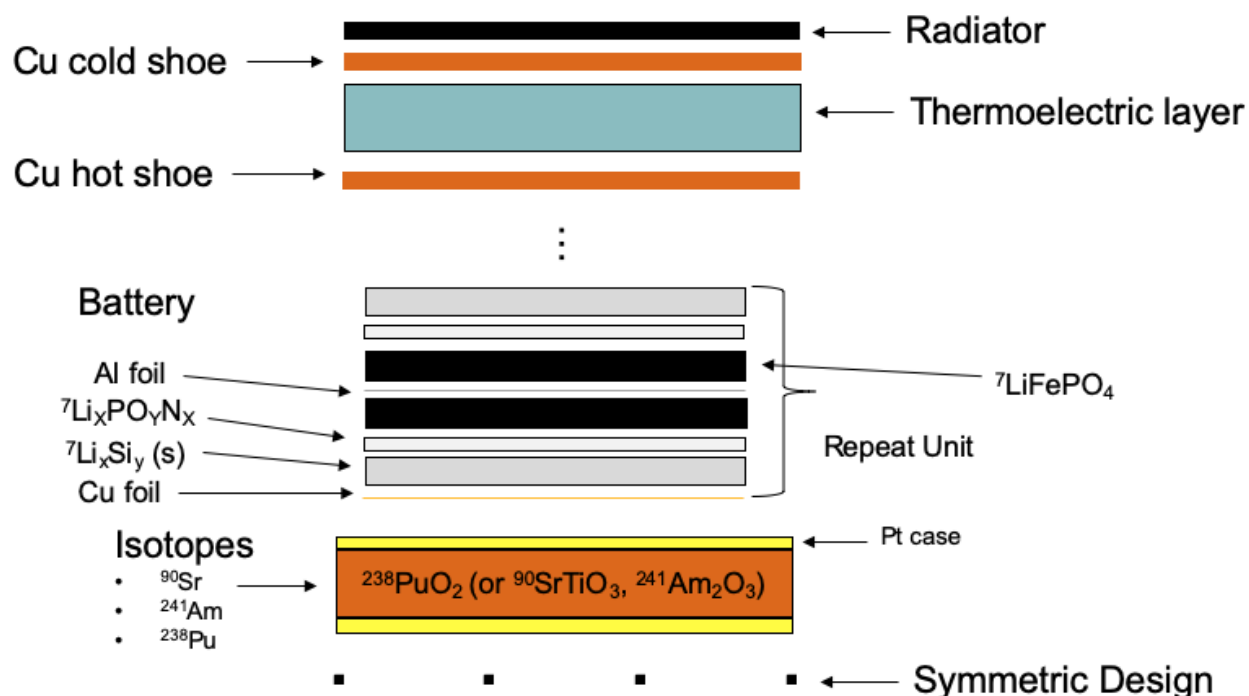


Figure 16. Version 1 of the APPLE concept, with the radiation hard battery sitting between the isotope core and the thermoelectrics. This version of the battery used high temperature materials for the anode and cathode.



these materials typically have a lower ion conductivity than the organic solvents plus lithium salts used in conventional Li-ion batteries. While extensive collective research efforts are underway to develop room temperature solid state ceramic electrolytes, the nature of the APPLE application opens up a wider range of feasible temperatures. As noted these solid state ceramics typically have acceptable ion conductance (while remaining electrically insulating) above 60°C. The high ion conductance at these temperatures combined with having the radiator surface at a temperature that can be still used as a heat source for other vehicle components allows for the optimized performance from APPLE for both power generation and heating.

The maximum battery material temperature was a significant constraint for the isotope type, geometry, and thermoelectric conversion, as lithium metal (m.p. 180°C) anodes could not be used for a battery in close proximity to the isotope heat source, and the higher energy density layered cathode materials like LiCoO<sub>2</sub> (LCO), LiNi<sub>x</sub>Mn<sub>y</sub>Co<sub>1-(x+y)</sub>O<sub>2</sub> (NMC), and LiNi<sub>0.84</sub>Co<sub>0.12</sub>Al<sub>0.04</sub>O<sub>2</sub> (NCA) would decompose during cycling from exposure to a temperature of 400°C, in the same reaction that drives Li-ion thermal runaway reactions, with spontaneous release of oxygen and heat when the cathode material is in its charged state. This lead to the choice to use a silicide anode, Li<sub>x</sub>Si<sub>y</sub>, and an iron phosphate (LFP) cathode, with a higher thermal stability, though reduced energy density compared to a lithium metal anode and a layered cathode in the initial radiation hard battery design.

The target temperature of 400°C was derived from the TEMs targeted in the design, PbTe for the n-type leg and a segmented design with TAGS and PbSnTe for the p-type leg for the Phase I design simulations. These materials have extensive heritage in NASA RTG mission, being used in the MMRTG and SNAP designs, and powering missions such as Mars Science Laboratory, Perseverance, Pioneers 10 and 11, and the Viking missions. The maximum temperature limits for these materials are 800 K for the n-PbTe, and for the p-TAGS, and 675 K for the p-PbSnTe, as shown in Figure 17<sup>37</sup>. The lower p-PbSnTe operating temperature can operate in this design as it is below the p-TAGS in the p-leg design. The maximum operating temperature from this

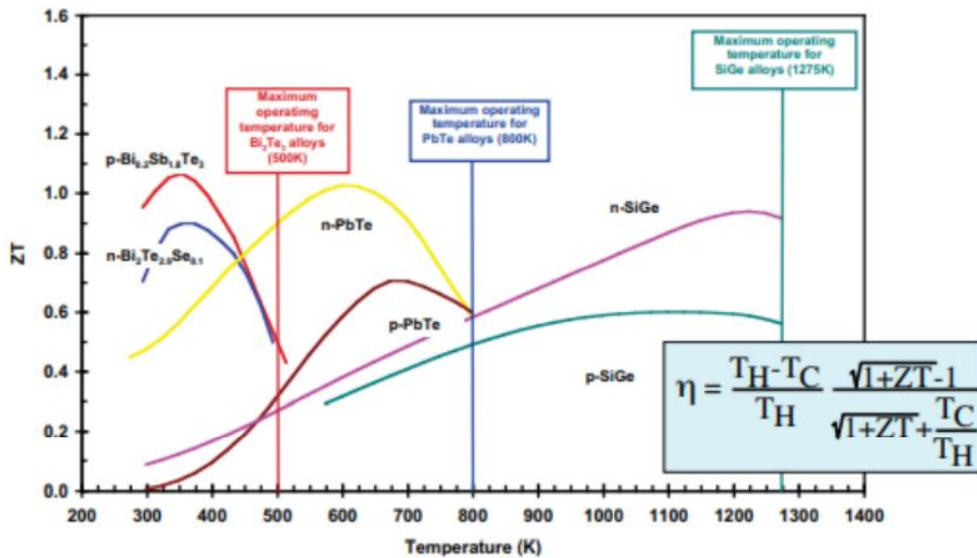


Figure 17. ZT values for a range of thermoelectric materials. The TEMs targeted in phase I were the TAGS system, with optimal ZT values in the 600-700K range, from Calliat, et. al., 2013.

figure as well as the battery material constraints was then less than 400°C, and the minimum temperature was set to greater than 60°C.

## 4.2. Isotope Properties

$^{238}\text{PuO}_2$  was chosen as the primary radioisotope material at the core of the APPLE design.  $^{238}\text{PuO}_2$  decays primarily through alpha emission to generate heat at beginning of life (BOL) of 0.50 W/g and at end of life (EOL-15y) at 0.45 W/g for the oxide.<sup>38</sup>  $^{90}\text{SrTiO}_3$  and  $^{241}\text{Am}_2\text{O}_3$  are two isotope materials commonly considered as alternative options to  $^{238}\text{PuO}_2$  as the radioisotope material, but have effectively lower heat output per gram at 0.46 W/g for  $^{90}\text{SrTiO}_3$  and 0.10 W/g for  $^{241}\text{Am}_2\text{O}_3$  at BOL, and 0.32 W/g for  $^{90}\text{SrTiO}_3$  and 0.10 W/g for  $^{241}\text{Am}_2\text{O}_3$  at EOL.<sup>39</sup> These thermal outputs were used for the thermal simulations for this study. This study primarily considered the  $^{238}\text{Pu}$  case due to the radiation penetration and capture depths discussed in the Radiation Simulations section above in addition to the higher mission thermal output. However, the general lessons of the thermal simulations apply across the different isotopes in terms of thermal output if the isotope masses are scaled to an equal thermal output, ignoring any capture length or materials. For  $^{241}\text{Am}$ , as discussed above, this capture material can be performed by increasing the existing cladding of the isotope, while  $^{90}\text{Sr}$  would require a much larger additional component for radiation capture, especially for the beta particles.

## 4.3. Thermoelectric Design Considerations

The electric performance of the APPLE design will depend on the TEM materials and design, with their constraints of conversion efficiency based on the equilibrium hot and cold shoe temperatures. Figure 18 is a thermoelectric device configuration with the hot and cold shoe locations, and heat transport from the heat source to the heat sink.<sup>40</sup> Copper was used as the hot shoe and cold shoe material for this design for its high thermal conductivity. Initial TEM materials were based on a single material for the n-type leg and two (segmenting) legs for the p-type leg. As the design matures, cascading or segmenting of the TEM materials for both legs

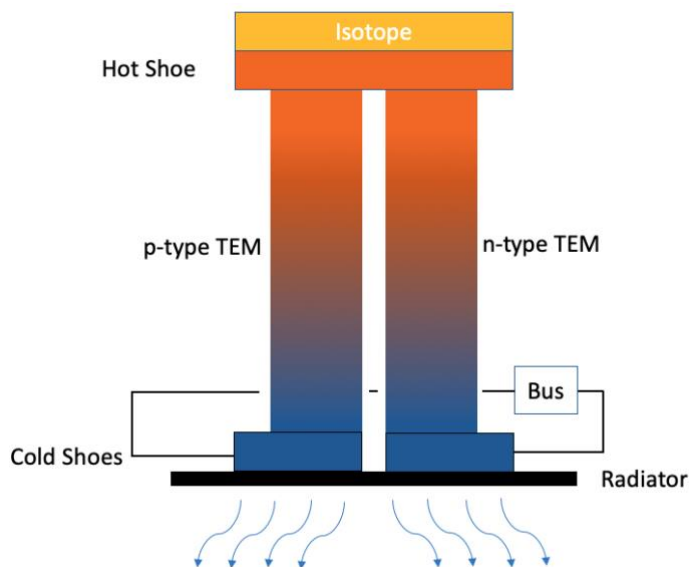


Figure 18. Thermoelectric junction scheme, showing the heat transport in the n- and p-type materials between the hot and cold shoes.

may be the option for best performance. Cascading or segmenting designs will require multiple materials for n-type and p-type legs. Figure 19 presents cascaded and segmented TEM designs.<sup>41</sup> The cascaded/segmented TEM are more efficient as the materials in the n- and p- legs operate in the temperature range in which they possess the highest ZT values. Both types of TEM designs maximize ZT value as well as maximizing temperature drop from the hot shoe to the cold shoe.

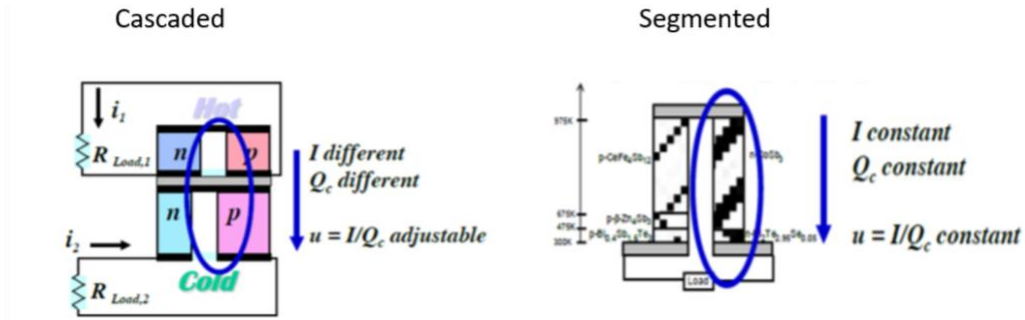


Figure 19. Cascaded and segmented thermoelectric device designs. From Fleurial, et. al., 2011.

The efficiency of thermoelectric conversion depends on the equilibrium  $\Delta T$  between the hot and cold shoes and the ZT of the thermoelectrics, and scaled to the total heat passing across the thermoelectric junction. To this end, insulation is needed to surround the isotope heat source and the thermoelectrics to avoid thermal losses to the environment before passing fully through the thermoelectric junction. Figure 18 shows the heat flow through the TEM between the hot and cold shoes through the n- and p-junctions.<sup>42</sup> Research on the best materials to compliment the TEM to minimize heat losses focused on aerogels and multi-layer insulation (MLI). The work presented uses aerogel as the insulation material due to its ease of application. The aerogel used had a thermal conductivity of 0.015W/mK, and a density of 0.1g/cm<sup>3</sup>. The effective thermal conductivity for MLI (not used in this analysis, but likely for future designs) depends on the number of layers and the emissivity of the material. The lower the emissivity and the more layers, it does not take much to be lower than the aerogel thermal conductivity. MLI would help to minimize heat losses and mechanical assembly and function, but the design would be more complicated for the initial design concept analysis. A combination of both aerogel and MLI would likely be the optimum design to minimize heat losses and ease of fabrication.

The conversion efficiency of the TEM module is a function of both the thermoelectric materials and the equilibrium temperature delta across the hot and cold shoes. Equation 2 and Equation 3 present the conversion efficiency equation. The efficiency ( $\eta$ ) is derived directly from the properties and the temperature drop across the shoes. The Seebeck coefficient (S), the electrical resistivity ( $\rho$ ), and the thermal conductivity ( $\lambda$ ) are the properties of the TEM module that describe its performance.<sup>43</sup>

Equation 2

$$ZT = \frac{S^2 T}{\rho \lambda}$$

Equation 3

$$\eta_{max} = \frac{T_{hot} - T_{cold}}{T_{hot}} \frac{\sqrt{1+ZT} - 1}{\sqrt{1+ZT} + \frac{T_{cold}}{T_{hot}}}$$

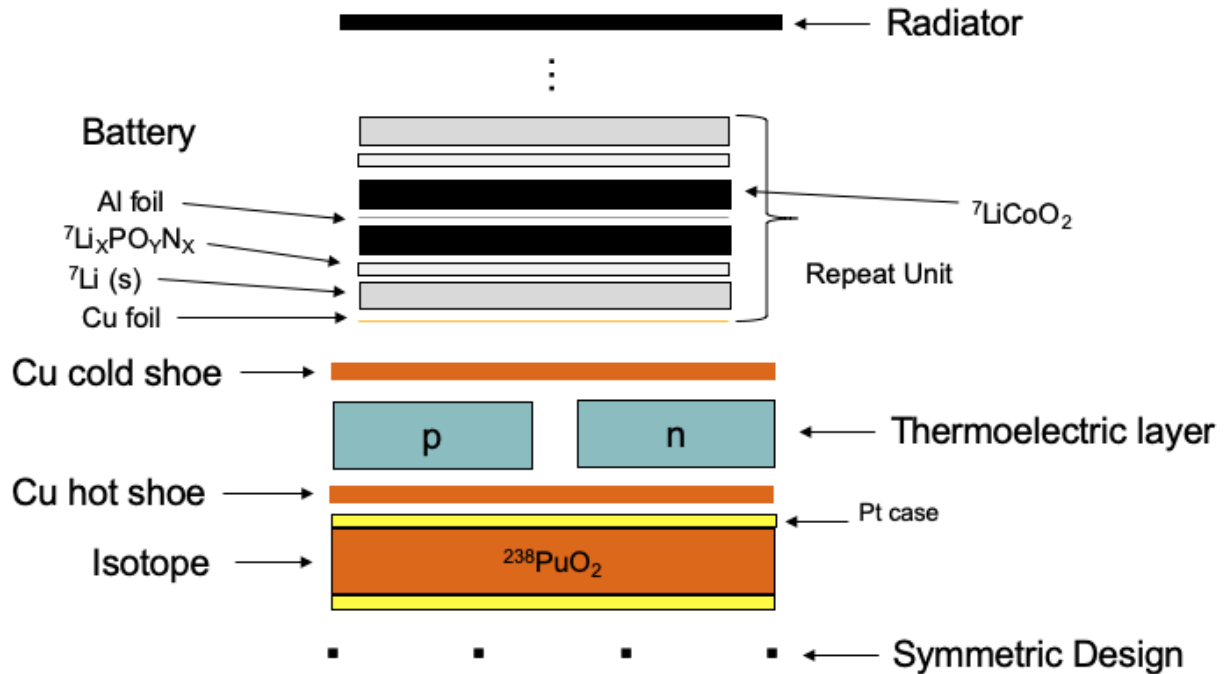


Figure 20. Version 2 of the APPLE design, with a battery-on-radiator design to reduce thermal constraints on the battery materials.

The original APPLE design had a battery on isotope configuration (Figure 16). Initial analysis and design discussions resulted in modifications to the initial design. The materials limitations imposed by the high temperature at the battery/isotope interface ( $400^{\circ}\text{C}$ ) in conjunction with the radiation simulations showing essentially no radiation escaping outside of the isotope oxide (using  $^{238}\text{Pu}$ ) lead this study to modify the design to a battery on/as radiator design. The modified APPLE design had the battery between the cold shoe and the radiator surface, resulting in better thermal constraints on the battery, as well as the thermoelectric materials, shown in Figure 20. While this design minimized the role of the battery as a radiation shield it allows the battery design to target the  $60\text{--}80^{\circ}\text{C}$  temperature range, which allows for optimization of the  $\Delta T$  of the thermoelectric conversion and but still keeps the battery temperature in a range where the electrolyte conductance is acceptable to rapid discharge performance. In addition, by making the battery the radiator mass for APPLE, a larger radiator could be used than is normal in RTG systems, because the radiator mass was serving another purpose, in this case, energy storage. A large radiator will increase the  $\Delta T$  for energy conversion and increase the TEM efficiency for a given ZT.

Figure 21 shows a comparison between the TAGS system and the SiGe system used in the MMRTG (TAGS) and the GPHS-RTG (SiGe). While the two systems used very different  $\Delta T$ s, the heat-to-electricity conversion efficiencies were similar, primarily due to the different ZT values of the thermoelectric materials used. The TAGS/PbTe based MMRTG had an efficiency of 7.0% based on a  $\Delta T$  of 315K and similar radiator profiles. The large radiator (25:1) of APPLE should enable highly efficient heat to electricity conversion.



	N-PbTe	P-TAGS/PbSnTe	N- GPHS RTG SiGe	P-GPHS RTG SiGe
Average ZT	0.90	0.84	0.69	0.41
Maximum Operating Temperature	800 K	675/800 K	1275 K	1275 K
Couple Efficiency/ Design	7.0% [800 to 485K]  Conductively coupled		7.5% [1275 to 575 K]  Radiatively coupled	
System efficiency	6.2 %		6.3 %	
Application	Multi-Mission RTG  2.8 W/kg		GPHS-RTG  5.1 W/kg	

Figure 21. TEM space heritage materials with efficiency and temperature application, comparing a TAGS system to the SiGe system. The TAGS/PbTe MMRTG has an efficiency of 7.0% for the  $\Delta T$  of 315K. From Calliat, et. al., 2013.

Figure 22 presents several design arrangements considered for the TEM legs within the APPLE tile. A key concern was allowing for sufficient distance for the heat transfer along the TEM. The thermal conductance (thermal conductivity\*leg cross-sectional area)/(leg length) describes the heat flow from the hot shoe and cold shoe for their temperatures. The thermal conductance for the individual thermoelectric materials and the heat to be transferred dictated the required lengths of the TEM legs. The values used for the analysis was 2.0 W/m-K for the thermal conductivity for both the n-and p-legs, with the thermal conductivity a function of temperature in the analysis. Phase II analysis will include the temperature dependence and variation between the n- and p-legs. The values for the leg cross-sectional area and the leg lengths were fixed for this analysis. In the first APPLE design there was a single large isotope source in the device, and this combined with the material thermal conductance gave very long TEM leg lengths, which required legs that were longer than the desired tile thickness. This lead to an initial design with the thermoelectric legs laying down in the plane of the device. With the TEM legs in a horizontal position, or the legs being of any horizontal position between the hot and cold shoes gave rise to excessive heat losses for this APPLE design, even with high efficiency thermal insulation. The design was modified by separating the isotope core into smaller units (4x), so the leg length parameters could be brought under the 1 cm tile target length. The traditional TEM leg (vertical) orientation minimizes heat losses but does have a design finite leg length. With the  $\Delta T$  requirements and the minimum battery temperature of +60°C, there can be some future optimization of the TEM leg length, area, and design, and thus the overall tile thickness, but likely not significant reductions in leg lengths without using TEMs with different thermal conductances.

#### 4.4. PATRAN Thermal Simulations

A PATRAN finite element model was built in Phase I was used to simulate the APPLE power conversion system, including charactering the APPLE Core surface temperatures, hot and cold shoe equilibrium temperatures, thermal to electrical conversion efficiency, and the battery heat

transport dynamics. The power conversion system model included the radioisotope cores, the thermoelectrics, the radiating surface (including interaction with vacuum space and the heat transfer to internal components), and an optimizable set of insulation materials.

SINDA/FLUINT<sup>44</sup> was used for the analysis and optimization model and is based on finite difference mathematics using temperature dependent materials properties. The tool utilizes the thermal transport coefficients, heat capacities, interfacial transport dynamics for the thermoelectric, the insulating material, the radiator, and estimates of the battery properties. The model utilized a high nodal count to ensure fine grained simulation results and to minimize edge interactions and errors. The APPLE design was matured by using the SINDA/FLUINT analysis to simulate the thermal/electric response with varying radioisotope decay heat (varying mass/volume of the isotope core).

Design boundary condition constraints were driven by the radioisotope decay heat under BOL and EOL conditions. The heat sink temperature for space was at 3 Kelvin. For simulations the tile was simulated as single sided, with one face (radiator) facing space and the other side considered to be a zero net heat transfer interface. This is appropriate for simulating the system as double sided, since an identical device back to back on this face would result in zero net heat transfer. For a single sided device, the applicability of the single sided simulation would require insulation, the efficiency of which could be used to account for any heat losses to that direction by reducing the assumed heat output of the isotope core. A value of 0.9 was used for the radiator emissivity and a radiator view factor of 1.0 to space. This view factor accounts for an unobstructed view of space, and the best case scenario for applications where only radiation to space is used for heat disposal. For designs where radiator heat is abstracted to heat spacecraft system components, the net heat flux from the radiator (regardless of heat destination) will need to be accounted for in determining the equilibrium temperature of the radiator. In these simulations, then, the heat deposition to space can be substituted with a total heat deposition to any source, and the thermal simulations will be agnostic to the heat destination. Full thermal simulations would be required for actual mission designs, accounting for radiator view factor,

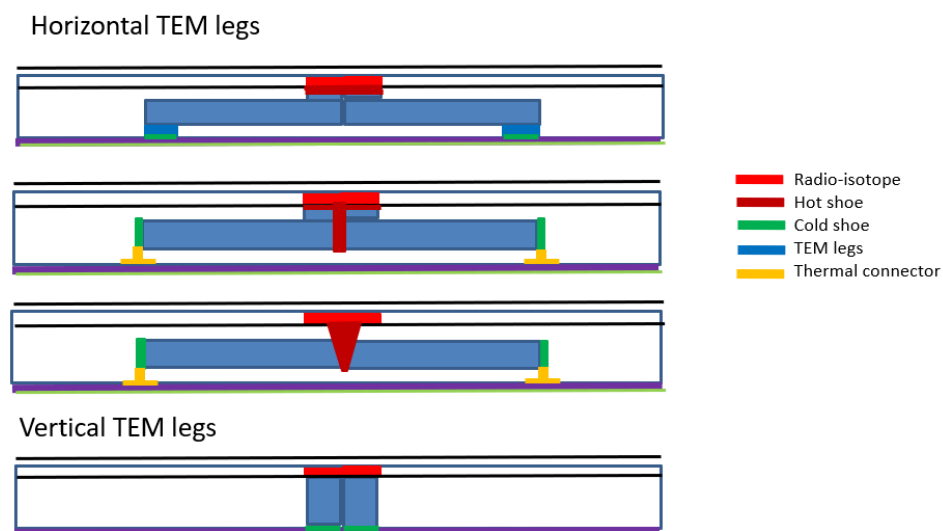


Figure 22. Thermoelectric design possibilities considered. Initial designs focused on in-plane TEM legs to achieve target radiator temperatures. The final design, with vertical legs resulted after reducing the size of the individual heat sources.



any heat transport to the vehicle, and radiator emissivity changes over life. This simulation is targeted for Phase II of this project, considering a Solar Gravity Lens mission vehicle design.

Simulations and geometric simplicity leaned towards a traditional concept with a distributed ratio between the hot/cold shoes and the radiator area. In addition, by keeping the TEM leg design similar to heritage designs, fabrication of the TEM legs will not require new methods or techniques. Figure 23 presents SINDA/FLUINT analysis PATRAN contour temperature plot of a unit cell of the APPLE design over a 5 cm by 5 cm area with a 1 cm<sup>2</sup> radioisotope square (0.5 cm thick) coupon at its center. This design had its maximum TEM (hot shoe) temperature below 800 K and the TEM (cold shoe)/radiator temperature at about 390 K. This unit cell only has heat radiating (one side) to space from the radiator. The sides of the unit cell are adiabatic, with silica aerogel accounting for the non-TEM volume.

The unit cell presents the heat flow (~87.5%) from the radio-isotope to the radiator being dominated through the TEM for the 2.9 W heat output from the isotope. 12.5% of the heat was still lost through the insulation and non-thermoelectric paths, and the unit cell produced 0.25 W electrical, for an efficiency of 8.6% for a  $\Delta T$  of 410K. The higher  $\Delta T$  in this APPLE design as compared to the TAGS/PbTe system in the MMRTG design allows for the 37% increase in heat to electricity conversion. The large radiator from the flat design of APPLE (25:1 area ratio

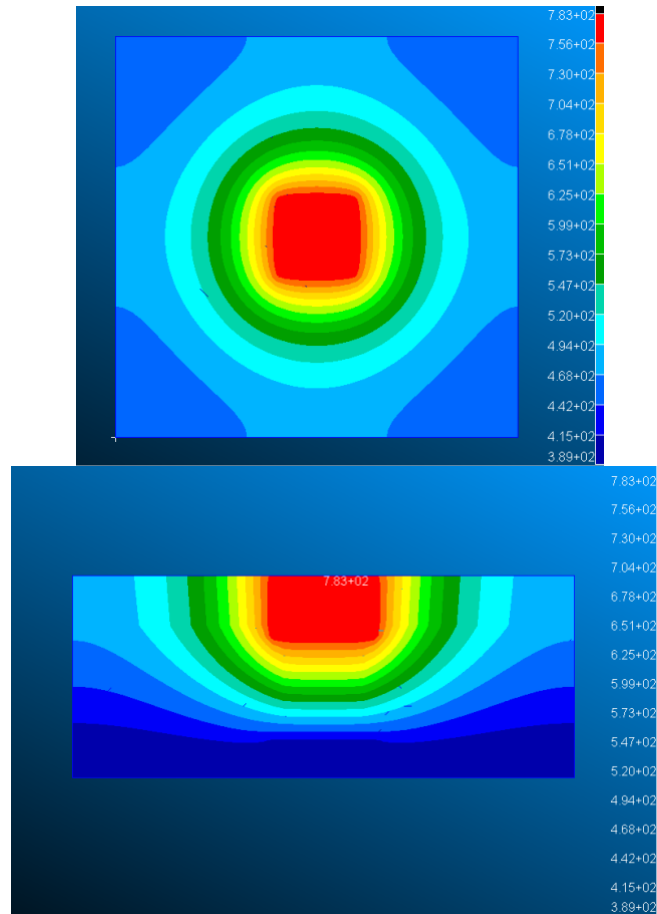


Figure 23. Temperature contour plot of a 1 cm<sup>2</sup> isotope core. Temperatures (K) at the isotope source were 800K and 390K.

between the isotope and radiator) allows for this high energy conversions. APPLE's multifunctional radiator, which is also serving as an energy storage device, allows for a large radiator without an extraneous mass. APPLE's tile form factor intended for distribution on the spacecraft surface or solar sail structure additionally benefits the power generation figure of merit.

The unit cell was multiplied by 4 to simulate the a tiled designed to produce at least 1 W electrical per coupon module per single side, the target for this APPLE design. Figure 24 presents the current APPLE design distributed heat sources over a 10 cm by 10 cm square area (100 cm<sup>2</sup>) for a single-sided or double-sided design. This design has four 1 cm<sup>2</sup> radioisotope cores evenly distributed throughout. This distribution of the radioisotope coupons allows the radiator surface to approach a uniform temperature. The distribution design allows the maximum heat input while keeping the maximum temperatures for the TEM within limits. Figure 25 presents the electrical power produced varying the radioisotope thickness for a single-sided and double-sided design. This allows for analysis of the power output of different thicknesses of isotope at beginning and end of life. This isotope is the <sup>238</sup>Pu, with its 87.7 year half-life, and the End of Life time for this was taken to by 15 years. It should be noted that 15 years is not actual end of life for an APPLE tile, as only 12% of the <sup>238</sup>Pu will have decayed at this point, but it does represent a good determination of failure times for other systems in the mission vehicle.

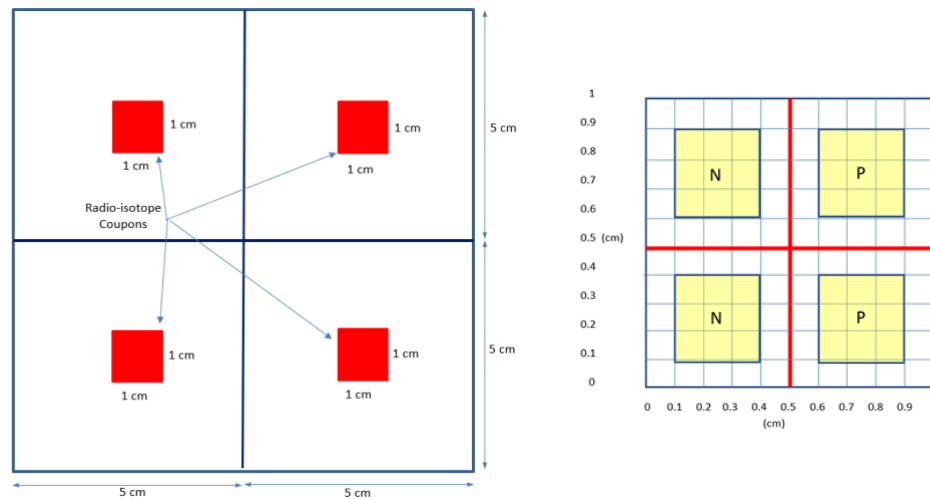


Figure 24. Left: Schematic with four radioisotope cores in a 10 x 10 cm tile. Right: the arrangement of the n-type and p-type legs for each isotope 1x1 cm square, covering 60% of the isotope interface.



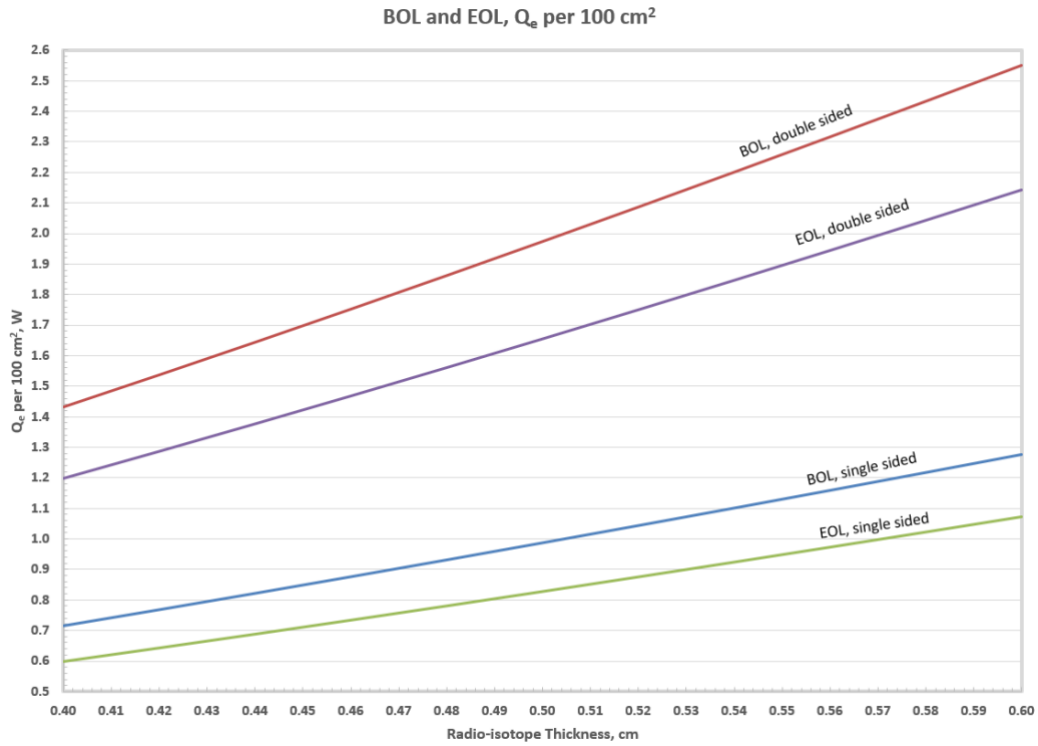


Figure 25. Electrical power production per tile at beginning and end (15-y) of life for single sided and doubled sided designs using 4 isotope cores.

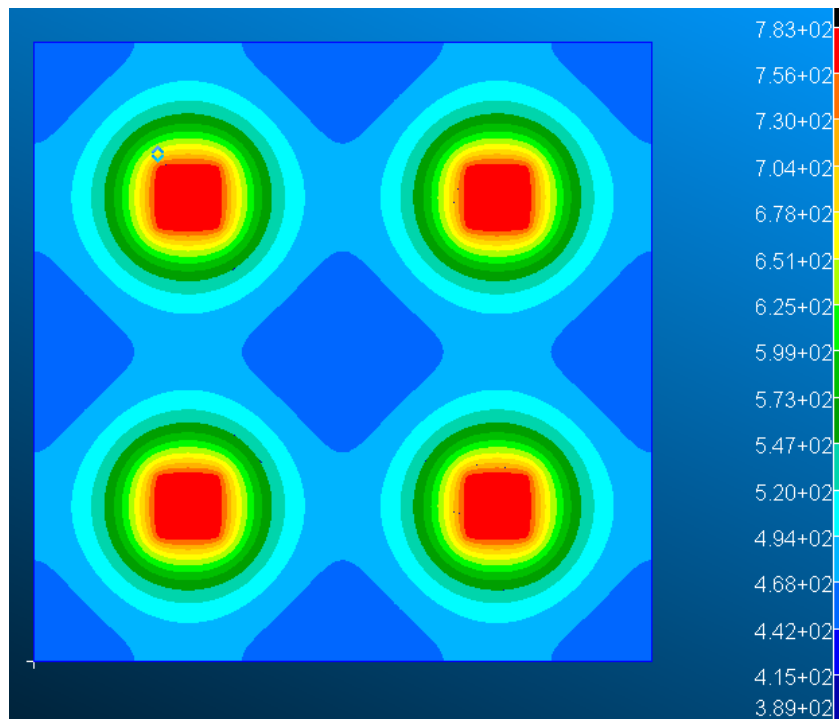


Figure 26. Top down view of the thermal profile with four isotope cores. Maximum temperatures are 783 K at the cores.

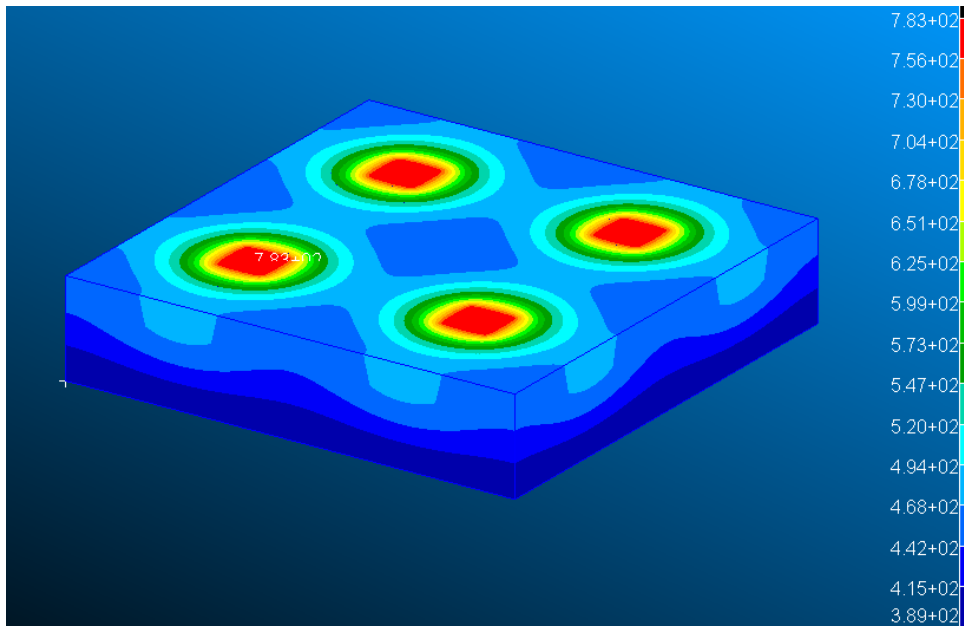


Figure 28. Isometric view of thermal profiles.

Figure 26 presents a single sided PATRAN contour temperature plots at a radioisotope thickness of 0.5 cm for an area of 100 cm<sup>2</sup> for a radioisotope top view and for an isometric view. This pattern can be repeated for larger tiles, but this 10x10 cm tile represents the single APPLE unit. Figure 28 shows an isometric view of the PATRAN contour temperature plot showing the uniform temperature at the radiator interface and the uniformity of the temperature gradient in

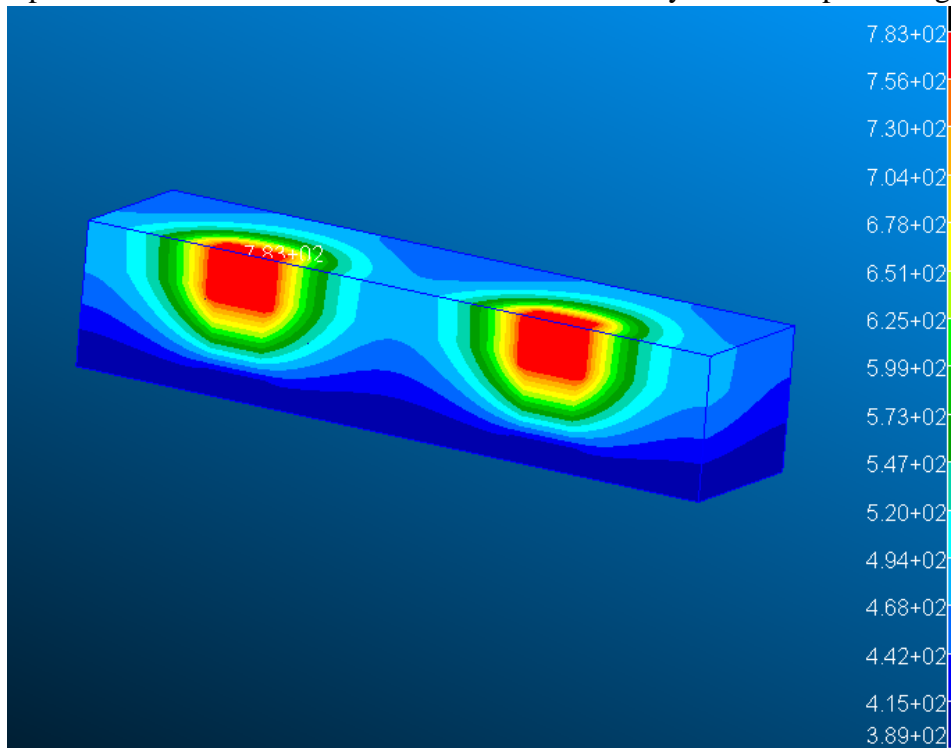


Figure 27 Contour temperature plot cross section showing (red) isotope cores, and the heat drop through the TEM to the radiator surface (bottom face).

the insulating layers. Figure 27 shows the cross section of the heat profile, with the 0.5cm thick isotopes having a uniform temperature gradient from the isotope cores through the thermoelectric materials directly beneath them. The distributed design can be improved for electrical energy production by minimizing heat losses and by getting better performing thermoelectric materials (higher ZT values). The current analysis used aerogel as the insulation material for the APPLE design. Heat losses can be minimized by incorporating MLI with the aerogel where applicable from this first design, which only used aerogel in the non-isotope, non-TEM volumes of the device. Currently, these thermal losses are ~12.5% for this design, representing the thermal loss through the insulation.

#### 4.5. Next Steps in Phase II

The initial design with analysis shows that the APPLE concept can be used in many applications. These applications include satellites, planetary vehicles, stationary applications, localized heat and power spacecraft needs, etc. Essentially any application where sunlight is not an option for power, and where there is the capability to effectively dissipate heat to the environment (i.e. not Venus, sun side Mercury).

The TEM can be improved by next generation novel thermoelectric materials being developed such as an improved SiGe, skutterudites (SKD), LaTe, Zintl, etc., which can have higher figures of merit (ZT) values and wider/higher temperature application. Figure 29 presents some of the ZT values versus temperature for some advance thermoelectric couple technology materials.<sup>45</sup> Advanced materials give the APPLE concept the ability to increase the thickness of the radio-

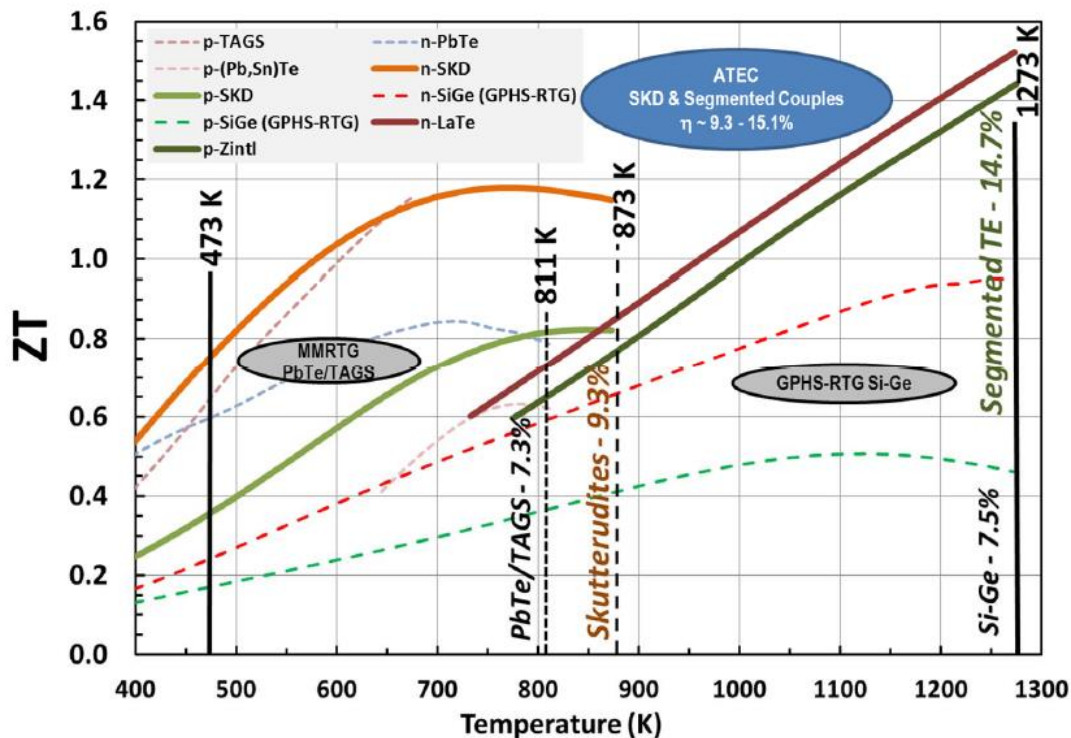


Figure 29. Advanced thermoelectric material couple technologies. Skutterudites offer a wider hot shoe operating range and increased efficiencies, from Otting, et. al., 2015.

isotope material for higher electrical energy. This leads to higher temperatures with modifications to the TEM n- and p- leg lengths to optimize the design.

Phase II of this project will work with skutterudite materials in JPL's Thermal Energy Conversion Materials Research Group for development and fabrication of more efficient TEM couples. In a new design, the target temperatures and design dimensions will likely be adjusted, but due to the higher efficiencies this next generation of device will exceed those simulated in Phase I.

## 5. Mission and Application

### 5.1. Introduction

The APPLE architecture has three fundamental attributes. 1) It generates power, 2) it stores energy and 3) it provides heat that can be used to keep spacecraft components warm. These attributes make APPLE most useful for space missions where solar flux is lax, and temperatures fall below the operational requirements for instruments requiring additional power for component heating. The missions could be in-space missions and/or off-world grounded missions (e.g., planets, asteroids). In the thermal simulations above, the radiator was simulated as transmitting energy to space to generate the required  $\Delta T$ , but the radiator can function through other heat transport mechanisms like conduction and convection in addition to radiation. This means that APPLE can be adapted to other environments than deep space. For example, an APPLE powered mission could be used in a rover on a rocky planet or swimmer on Enceladus, with heat transport to a wispy atmosphere or a liquid environment. The thermal transport would need to be simulated for each of these environments, and would give rise to different radiator designs to maintain desired battery temperatures and hot shoe-cold shoe  $\Delta T$ s.

### 5.2. APPLE Tile Designs

APPLE in the design presented here has two fundamental concepts. One is the double sided tile, with radiative surfaces intended to face deep space for heat rejection. This version of APPLE would be installed on booms or extensions from the vehicle in a similar design to existing vehicle solar arrays. The second design would see APPLE as single sided tiles placed on the outer surface of the vehicle. This single sided concept would use multi-layer insulation on the isotope side of the tile to prevent heat loss to the environment rather than having the heat transported through the thermoelectrics. The heat post thermoelectric can either be radiated to space like in the double sided design, or could be transported to other vehicle components through the use of heat pipes. Only the  $\Delta T$  between hot and cold shoes matter for energy conversion, whether that cold shoe is in radiative equilibrium with the background of space or in a steady state heat transfer condition to the spacecraft.

Regardless of the manufacturing details, APPLE has flexibility in its design, in that as a half-tile, it could be attached to curved sections of a spacecraft bus, much like a photovoltaic but not necessarily in a flat configuration. In this type of application, the faces of the full-tile are space-facing to remove the excess heat. Moreover, as space electronics prove to be more rad hard in the future, one can conceive that some space systems may be designed around an APPLE power system where it serves as a structural component, i.e., “build the spacecraft or instrument on top of the power system.” Alloys of the lithium anode with aluminum provide improved mechanical strength (776 MPa)<sup>46</sup>. As a comparison, the tensile strength (the maximum amount of tensile stress before failure, i.e., breaking and permanent deformation) of structural steel is 400 MPa and 841 MPa for carbon steel. Consequently, APPLE could expand the design space for spacecraft manufactured on ground or in space.

In the current design, APPLE is configured as a tile, but because of its layer-by-layer design, it could also be shaped as a curved surface, to be a “wrap” of sorts. The anode and cathode

sections of APPLE could easily be made conformal to the surface which it is to be attached. Because the isotope/thermoelectric interfaces do not take up much area, they can also be made to conform to the curvature of the anode/cathode sections and be integrated into the sandwich design. The solid-state electrolytes may be less flexible (e.g. LiPON ( $\text{Li}_x\text{PO}_y\text{N}_z$ ), LISICON ( $\text{Li}_{14}\text{Zn}(\text{GeO}_4)_4$ )) but they can be deposited on a curved substrate surface (e.g. cathode/anode) or be made thin enough that they are inherently adaptable to a variety of shapes and surfaces.

### 5.3. APPLE Powering the Solar Gravity Lens Mission

The recent release of the National Academy Astro2020 Decadal Survey report places a focus on identifying and characterizing exo-planets. At the level of a single pixel “image”, the proposed *next great in-space observatories* should provide much insight, but to gather a multi-pixel image of an exoplanet, there is only one practical approach. This approach is in the conceptual design phase and funded by the NIAC Phase III (Direct Multipixel Imaging and Spectroscopy of an Exoplanet with Solar Gravitational Lens Mission, S. Turyshev, JPL).<sup>47</sup> The Solar Gravity Lens (SGL) mission attempts to send a group of spacecraft to 650 AU, at which point, on board imagers can harness the  $10^{10}$  level of optical magnification permitted by the Einstein gravity lens created by the Sun.<sup>48</sup> It is a challenging mission where the APPLE attributes play a significant role to make the mission feasible. First, the SGL mission is encumbered by the need for power to maintain a communication link at several 100 bits/s from 650-900 AU. In addition to this power draw, calculations show that in the science phase of the mission, the SGL satellites must continually thrust (albeit small) to maintain a trajectory path that appears like a wobbly corkscrew with accelerations that reach  $9 \text{ m/s}^2$ . This trajectory follows the location of the SGL which is affected by the wobble motion of the Sun (i.e., the lens) and the perturbative forces on the exo-planet induced by possible wobble of the host star. Current analysis using EP thrusters (e.g., Morpheus FEEP) show that a power requirement of 100-150  $\text{W}_e$  (EOL) is needed for the 40-year mission. While this is possible via RTGs or a Brayton power system (which is more energy conversion efficient but has moving parts, a substantial risk over such a long mission) they are heavy (e.g., NASA’s Apollo Lunar Surface Experiments package SNAP-27 power supply provided 75  $\text{W}_e$  and weighed 20 kg).

The mass of the spacecraft bus is a strong constraint for the SGL mission. To reach 650 AU within a human scale generation, the SGL spacecraft must travel  $> 20 \text{ AU/yr}$ . Current propulsion technologies can barely reach  $\frac{1}{4}$  of these velocities. However, analysis shows that if each subsystem were to be partitioned to mass budgets on the order of 5-10 kg, it would permit the use of solar sail propulsion coupled with a close solar perihelion transit ( $\sim 10$ -15 solar radii). Velocities of up to 60 AU/yr (0.1% of the speed of light) and above are permissible, if the solar sailcraft can survive a 2-5 solar radii transit. The development of a robust solar sail material technology that would survive the extreme face-on temperatures  $> 100^\circ\text{C}$  is under investigation by another NIAC Phase II program (Extreme Solar Sailing for Breakthrough Space Exploration, A. Davoyan, UCLA).

The SGL mission requires flying an ensemble of nanosatellite class spacecraft, all individually accelerated to high velocity but flying in formation and at an orbit near that of Earth conducting in-space docking maneuvers, without the sails, to assemble a mission-capable spacecraft. Concurrent Engineering Methodology (CEM)<sup>49</sup> analysis of the SGL mission shows that APPLE

can play key role by first individually powering the maneuvers of the nanosatellites and after the in-space aggregation and assembly providing the necessary power for the 40-year mission. Using the CEM tool, and existing spacecraft systems technologies for the power system, the initial parsing of the spacecraft subsystems into nanosatellite class units produced an aggregate vehicle that combined 7 nanosatellites (3-6U volume each) but with a net mass varying from 180-250 kg, too large to be used with the proposed solar sail propulsion system. The largest mass subsystem was the Brayton power system and radiators. In addition, the Brayton system required additional batteries for the peak power segments of the mission.

A re-analysis of the SGL mission bus using APPLE tiles produced a mission-capable satellite that is an assembly of 6 pancake-shaped nanosatellites, instead of 7. Each nanosatellite is approximately 1 m in diameter and 10 cm thick with an aggregate mass of 126-180 kg (40 or 45 year mission, 5-10 year science phase). A mass savings of 54-70 kg (~30%). An external view of the spacecraft bus is shown in Figure 30 from the end view of the primary telescope mirror (minus the boom arm which holds the secondary mirror). The figure also displays the numerous EP thruster nozzles necessary to conduct the continual corkscrew trajectory motion while maintaining nano-arcsecond precision attitude. Given a 10x10 cm<sup>2</sup> tile area, it is possible to mount up to 24 half-tile APPLE units around the circumference of each pancake shaped nanosatellite. The total power generation capability on each nanosatellite is ~ 28 W<sub>e</sub> and nearly 120 Wh of storage (at 1.17 W<sub>e</sub> BOL per half-tile using a 0.6cm thick isotope and 5 Wh of storage per tile) with a mass burden of 1.8 kg. Because the SGL mission-capable spacecraft is an assembly of 6 nanosatellites we arrive at a total power capability of ~ 168 W<sub>e</sub> BOL and 720 Wh of storage. To generate 150 W<sub>e</sub> BOL using a SNAP27 RPS would have a mass burden of 40 kg. A turbo-Brayton system (Creare Corp.) would weigh ~14 kg but carry the increased risk of moving parts over the long duration mission. For the equivalent power, the estimated mass is 10

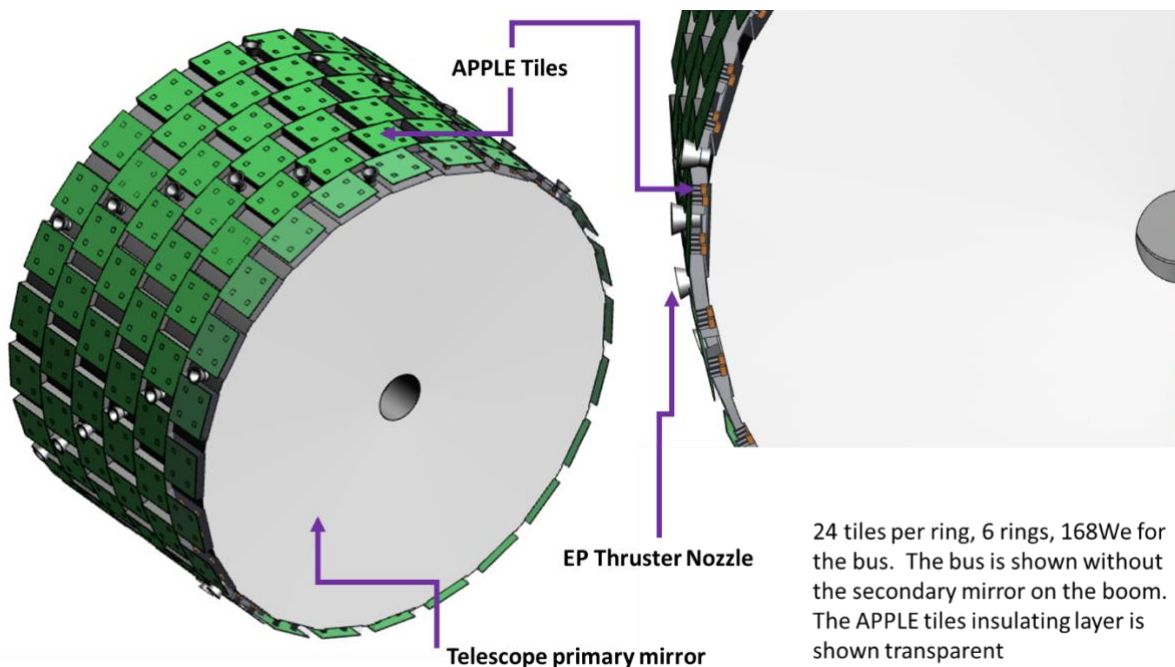


Figure 30. An SGL vehicle concept using single sided APPLE tiles around the circumference for power, energy storage, and heating.

kg using the APPLE architecture. In addition, a SNAP27 style RTG would require more  $^{238}\text{Pu}$  due to the lower  $\Delta T$  of that system compared to APPLE. As seen in the Thermal Design section, the large, multifunctional APPLE radiator creates a larger  $\Delta T$  and a corresponding increase in energy conversion, 37% in the example design studied here. This leads to a substantial reduction in the radiological risks of launching  $^{238}\text{Pu}$  as well as extending the  $^{238}\text{Pu}$  stockpile for additional missions.

Additionally, unlike the SNAP27 or the turbo-Brayton which have no innate battery storage capability, the SGL mission capable spacecraft based on the APPLE architecture carries  $\sim 720$  Wh of storage (for the 168 W<sub>e</sub> BOL). An estimate can be made of the additional mass savings in not carrying batteries. Using current nanosatellite battery technology and data from the “CubeSat Shop” and “Gomspace”<sup>50</sup> 10 Wh of energy storage carries a mass  $\sim 50$  g at the cell level. At 720 Wh of storage availability an additional mass savings of 3.6 kg is estimated in the APPLE design because the battery is integral to the power source. Additionally, the batteries would need to be tightly thermally regulated in either the Brayton or SNAP designs to keep them optimally functioning over the extended mission life. The built-in thermal regulation in the APPLE design, through the use of the solid state radiation hard battery maintains the battery in the optimal temperature over life without control systems or an additional power system cost.

## 5.4. Direct Spacecraft Thermal Regulation Through APPLE

Deep space missions might benefit from the generated heat that comes from an APPLE module for the sole purpose of keeping electronics temperatures within operational ranges. A single 10x10 cm<sup>2</sup> half-tile module generates 14 W<sub>th</sub> of heat. The Phase II effort of this NIAC, if received, will study attaching half-tile APPLE modules around a spacecraft bus to be used as means to regulate internal temperatures to advantage. In the future, spacecraft designs may incorporate concepts where the natural radiative loss into space are compensated by natural radiating sources with the goal of keeping internal temperatures within an operable range. While existing vehicle designs use temperature regulation mechanisms like heat pipes to distribute heat throughout critical systems, this is typically needed in RTG powered missions due to the requirement to keep the RTG away from the vehicle. RTGs are kept away from the main vehicle systems to allow their small radiators to have the best view of space for radiative transport. With APPLE’s large multifunction radiator and distributed thermal core design, the heat sources can be distributed on or even throughout the vehicle if proper thermal design is considered.

To simulate this concept, a thermal model was built to test the idea on a prototypical satellite “bus” that has two, end-to-end, 1 m diameter telescope imagers. We assume the satellite bus as a cylinder 70 cm in length and 1 m in diameter. We further assume that 70% of the outside cylindrical surface is covered by APPLE half-tiles at 800K (heat source) while the cylindrical front and back are kept at 70K (the radiation sinks into space). Without out any optimization the figure below shows the temperature distribution in this canonical cylinder. The model assumes the inside is a solid material (thermal conductivity  $\kappa = 0.26\text{W/mK}$ ), which would not be true in a real satellite model where the layout of the subsystems leaves some empty space and materials of varying thermal conductivities. The results of the thermal model, using 4 cm of multi-layer insulation material is shown in Figure 31. The temperature at the center falls to  $\sim 490\text{K}$  (217°C,



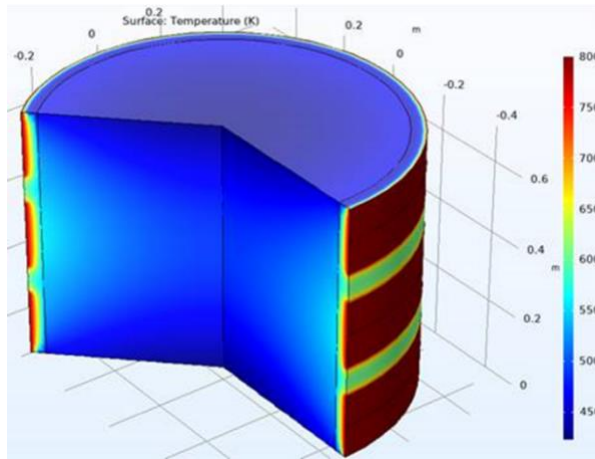


Figure 31. A thermal simulation of direct thermal regulation of a spacecraft through a distributed APPLE design.

in the realm of SiC electronics). The internal temperature could be further reduced to be within the operational range of conventional electronics by reducing the number of half-tiles on the outer surface or increasing the multilayer insulation thickness. This trade study coupled with use of canonical spacecraft structures will be a task in the Phase II, if awarded.

## 5.5. APPLE Antenna Structures

The APPLE architecture can be integrated into missions where it is placed on an extending boom or where it becomes part of a solar sail material, this could be at the attachment points to the sail boom structure or at selective locations on the sail material itself. The APPLE architecture could also be used as the reflector portion of an RF antenna. Under all these scenarios, a full-tile APPLE configuration would be appropriate with a factor of 2 gain in the generated electrical power and storage. The full tile consists of two half-tiles mated at the power core side leaving the battery layer as a thermal radiator (opposite the attachment scheme used for the SGL mission). The external layer of the battery material is a smooth surface and it could be coated with properties to better reflect RF energy or coated with reflective metallic material to mimic solar sail properties for propulsion. In the case of integration with an RF antenna, we demonstrate the scalability of the APPLE architecture (i.e., signal SNR is related to aperture size) by estimating the electrical power that can be produced when integrated onto an RF antenna. As an example, we take the small model of the L3Harris Corp. unfurlable Ka-band reflector which has 5 m diameter (Voyager spacecraft high gain reflector is 3.7 m dia). If 50% of the area were to be covered with APPLE full-tiles, then approximately 2.1 kW<sub>e</sub> could be produced by the antenna surface (coupled with 21 kWh of energy storage). The antenna surface would then act both as an RF reflector and power generator. The Voyager mission survived with only 410 W<sub>e</sub> (BOL) for the scientific packages it could carry. With the APPLE architecture, it could have carried more power demanding payloads. Another mission where electrical power is in demand is on spacecraft that carry synthetic aperture radar (SAR) payloads (e.g. NASA-ISRO, NISAR mission, planned launch 2023, which carries a SAR payload requiring 6.5 kW<sub>e</sub>). Further analysis has to be conducted, but the APPLE architecture could also possibly be implemented as part of the primary mirror of optical telescopes, not in the visible band, but in the deep IR (>50 μm, ~ 5THz), where the spectral irradiance from an 800 K blackbody source,

emissivity = 1, is more reasonable (a full-tile APPLE) is  $< 1 \text{ W/m}^2/\text{sr}/\mu\text{m}$ . This would be background signal of the captured light. THz spectroscopy enables observation of larger gas phase molecules (e.g.  $\text{CH}_3\text{CN}$ ). If Phase II is awarded, we will explore the types of in space observational missions that might be possible by integrating APPLE RPS into a large aperture antenna/mirror.

## 5.6. APPLE Powered Ingenuity Follow On

APPLE can also open up exploration to moons and worlds where photovoltaic power is limited by the distance to the sun or through day/night cycles. A lightweight modular system would enable a wide range of rover designs, smaller and more capable than currently possible when using the large monolithic RTGs. Already MSL and Curiosity have chosen RTGs for power generation on Mars, even though other Mars exploratory missions such as Ingenuity, the small helicopter, have chosen a photovoltaic approach, likely due to the large size of the available RTG technologies. If APPLE was used for an Ingenuity-like follow on mission, it could efficiently replace the solar array + battery power system, while multiplying mission operation. The incident solar irradiation in the Martian northern hemisphere spring and summer is  $2,000\text{--}5,000 \text{ Wh/m}^2\text{-sol}$ ,<sup>51</sup> and the  $0.0544 \text{ m}^2$  fixed Sol Aero IMM4J array<sup>52</sup> during these seasons can then optimally generate between  $24 \text{ Wh/sol}$  and  $60 \text{ Wh/sol}$ . In addition,  $21 \text{ Wh/sol}$  of Ingenuity's power budget is to heat the vehicle and the six Sony VTC4 cells ( $42 \text{ Wh}$ ) during the Martian night.<sup>53</sup> One 90s flight uses about  $10 \text{ Wh}$ , which with the heater survival power means even in the peak of summer missions must be limited to less than one per sol. An APPLE power system could use 7 tiles to generate  $8.4 \text{ W}_e$  ( $202 \text{ W}_e/\text{sol}$ ) and store  $35 \text{ Wh}$ , while generating sufficient waste heat to eliminate heater usage. The Ingenuity power system (array + battery) weighs around  $600\text{g}$ , and the 7 APPLE tiles would have a similar weight, around  $525\text{g}$ . If only  $5 \text{ W}_e$  is devoted to battery storage, an APPLE powered Ingenuity successor would be able to make at least 10 flights per day, regardless of season or time.

## 6. APPLE Development Path

### 6.1. Isotope Supply

Of the candidate RTG isotopes either considered or used in previous applications,  $^{238}\text{Pu}$  has the lowest shielding requirements due to its production of primarily alpha particles, with stopping lengths in common spacecraft materials like aluminum and carbon in the 10  $\mu\text{m}$  range, thinner the housing components of any component that may be radiation sensitive, much less the typical heavy metal isotope cladding, materials like Ir or Pt. In addition, the 87.7 year half-life means that for even long missions EOL power levels have not diminished much from BOL. Actually, power losses for Pu RTGs are dominated by loss of thermoelectric conversion efficiency rather than isotope loss, typically through reduction in the efficiency of heat transfer at the hot shoe junction through sublimation of the thermoelectric materials.<sup>54</sup>

DOE agreed with NASA to restart  $^{238}\text{Pu}$  production in 2013.<sup>55</sup> This production, occurring at Oak Ridge National Labs, supplied some of the  $^{238}\text{Pu}$  used in the Mars 2020 mission, the first Pu RTG mission since the MSL, and using the last of the available old  $^{238}\text{Pu}$  stockpile. Oak Ridge began new production in 2015, and has been increasing its  $^{238}\text{Pu}$  production, with a goal to produce 1.5 kilograms of  $^{238}\text{Pu}$  per year by 2026.<sup>56</sup>  $^{238}\text{Pu}$  is produced at ORNL from neptunium-237 which is irradiated in ORNL's High Flux Isotope Reactor (HFIR), transmuting the neptunium into  $^{238}\text{Pu}$ . The  $^{238}\text{Pu}$  is purified from the neptunium and converted to an oxide powder for RTG use. Currently, HFIR can irradiate up to 6,800 grams of  $^{237}\text{Np}$  every two to three months. Oak Ridge is currently building additional facilities to increase production to meet their 1.5 kg/y production targets. This 1.5 kg/y target when achieved can enable APPLE powered missions to deliver  $\sim 70\text{ W}_e$  per year in mission power, enough to launch one small mission each year, or one large mission about every 5 years. Increasing these production targets through expansion of the fabrication facilities will open up many more missions, though it is likely that the motivation for this expansion will need to be driven by new mission designs, such as those enabled by APPLE. In addition, DoD interest in *cis*-lunar applications using non-solar power has increased in recent years, including the use of  $^{238}\text{Pu}$  and other isotopes for heat and power generation.<sup>57</sup> This interest may lead to additional investment in isotope production beyond what has already been arranged.

Alternative isotopes to  $^{238}\text{Pu}$  can also be considered as well for power production. As stated above, APPLE is relatively agnostic to the isotope identity, as long as the radiation products can be captured without too much additional dead mass. While the extremely cheap and available  $^{90}\text{Sr}$  has fairly comparable thermal output compared to  $^{238}\text{Pu}$ , the highly penetrating beta particles would require a substantial increase in capture mass compared to  $^{238}\text{Pu}$ , needing around 1 mm of Pt cladding on the isotope core for thermal capture (not human effects shielding). In addition, the faster decay rate of the  $^{90}\text{Sr}$  would necessitate care to size the APPLE tile design to EOL power output for mission duration, as  $^{90}\text{Sr}$  at 15 years will drop to 70% of the thermal output of a comparable  $^{238}\text{Pu}$  system. Another isotope considered for RTG applications,  $^{241}\text{Am}$ , being targeted by ESA for RTGs is commercially available as well.  $^{241}\text{Am}$  has a radiation profile that includes more penetrating gamma rays, but these can be captured for thermal conversion in the Pt cladding material used in APPLE by increasing the material thickness to  $\sim 200\mu\text{m}$ , and so would not as much additional mass to enable use. However, the lower thermal output would result in needing more isotope mass to achieve similar temperatures to the  $^{238}\text{Pu}$  design, reducing

the power density of an Americium APPLE. Current production of  $^{241}\text{Am}$  is estimated at 1 kg/y from commercial sources in its uses in smoke detectors, moisture detectors, and terrestrial RTGs.<sup>58</sup> This can be more easily increased through the processing of reactor waste than  $^{238}\text{Pu}$  production.

## 6.2. APPLE Thermal Core Framework

At the center of the APPLE design is the Power Core, the RTG heart of each APPLE unit, consisting of a  $1 \times 1 \times 0.5 \text{ cm}$   $^{238}\text{PuO}_2$  tile encapsulated in a Pt cladding. This small heat source generates  $2.9 \text{ W}_{\text{th}}$ , allowing for a flexible design of the APPLE architecture that scales by adding multiple cores to form an APPLE tile and then multiple APPLES to supply the mission power needs. Currently, NASA uses the General Purpose Heat Source (GPHS), a  $^{238}\text{PuO}_2$  bolus clad in iridium which measures 9.95 cm wide by 9.32 cm deep by 5.82 cm high and weighs 1.44 kg and provides  $250 \text{ W}_{\text{th}}$  at beginning of life. This was the heart of the GPHS-RTG system that powered Ulysses, Galileo, Cassini, and New Horizons, and is used in the MMRTG for Curiosity and Perseverance. However, the large mass and high heat flux of this heat source means that smaller spacecraft would be unable to use an RTG based on this thermal core. In the example of a 6U cubesat sized vehicle such as MarCO that uses about  $17 \text{ W}_e$  at Mars would be unable to use a power system based on even a single GPHS. In addition, with the current target of 1.5 kg of  $^{238}\text{Pu}$  produced per year, this would allow for only a single GPHS produced per year. The larger flagship missions that used the GPHS in the past typically used up to 18 GPHS per vehicle (8 in MMRTG, 18 in GPHS-RTG), limiting flagship missions to one every decade or two. As the future of outer solar system exploration expands, more designs for small craft will need more flexibility in their power system design, and consequently a smaller thermal core. The APPLE Power Core, at  $1 \times 1 \times 0.5 \text{ cm}$ , generating  $2.9 \text{ W}_{\text{th}}$  can be incorporated into this design to allow for small craft to access RTG power, but also enable more frequent launches of missions past Mars with the current planned supply of  $^{238}\text{Pu}$ . In addition, the APPLE Power Core design can be the framework for future RTG missions, even outside of the APPLE. With regular production of this component, further designs can be made to incorporate it as a power or heat source, opening up vehicle design far beyond what can be done with the existing monolithic RTGs.

## 6.3. APPLE Power and Mass Designs

Using the thermal design simulations and the battery capabilities the projected power and energy storage densities can be calculated for the  $10 \times 10 \text{ cm}$  APPLE design. Table 3 shows the mass of the components of the APPLE core components. This design uses Pt cladding to capture the radiation from the isotope core. In the case of  $^{238}\text{Pu}$ , this will be  $50 \mu\text{m}$  of Pt, though more material is needed to capture the radiation emitted from the other isotopes. The thicknesses of the TAGS/PbTe thermoelectrics is based on the thermal conductivity of the TEM materials, and used a 60% total area coverage of the hot and cold shoes for the materials. This design has an efficiency of 8.7% based on a  $\Delta T$  of 410K.

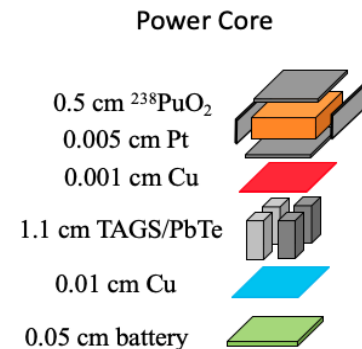


Figure 32. The APPLE power core using  $1 \text{ cm}^2$   $0.5 \text{ cm}$  thick  $^{238}\text{PuO}_2$  core clad in  $50 \mu\text{m}$  thick Pt on a thermoelectric stack.

Table 3. Thicknesses and masses of APPLE Power Core components for the  $^{238}\text{Pu}$  case

Power Core	Area (cm <sup>2</sup> )	Thickness (cm)	Density (g/cm <sup>3</sup> )	Mass (g)	Heat Output (W)	Power Output (W <sub>e</sub> )	Efficiency
$\text{PuO}_2$ tile	1	0.5	11.5	5.75	2.88	0.25	0.087
Pt cladding	1	0.005	21.45	0.43			
Cu hot shoe	1	0.001	8.96	0.009			
<b>Thermoelectrics</b>							
TAGS	0.25	1.1	6.5	1.79			
PbTe	0.35	1.1	8.16	3.14			
Cu cold shoe	1	0.001	8.96	0.009			
<b>Total</b>		1.61		11.13			

Similar calculations for  $^{90}\text{Sr}$  and  $^{241}\text{Am}$  in Table 4 and Table 5 show the weight penalties that come with having to use lower thermal output materials, and to account for the additional material to capture the radiation and convert it to heat. Increasing the Pt thickness to 1 mm for the  $^{90}\text{Sr}$  case and to 250 $\mu\text{m}$  for the  $^{241}\text{Am}$ , this should capture about 95% of the particles that leave the titanate and oxide in the Pt for heat conversion. This does not account for more fully shielding radiation for human exposure.

Table 4. Power Core thicknesses and masses for the  $^{90}\text{Sr}$  design, showing the substantial increase in Pt shielding mass.

Power Core	Area (cm <sup>2</sup> )	Thickness (cm)	Density (g/cm <sup>3</sup> )	Mass (g)	Heat Output (W)
$\text{SrTiO}_3$ tile	1	1.7	5.11	8.68	3.996
Pt cladding	1	0.1	21.45	18.8	
Cu hot shoe	1	0.001	8.96	0.009	
<b>Thermoelectrics</b>					
TAGS	0.25	1.1	6.5	1.79	
PbTe	0.35	1.1	8.16	3.14	
Cu cold shoe	1	0.001	8.96	0.009	
<b>Total</b>		2.90		32.5	

Table 5. Power Core thicknesses and masses for the  $^{241}\text{Am}$  design, showing the substantial increase in Pt shielding mass.

Power Core	Area (cm <sup>2</sup> )	Thickness (cm)	Density (g/cm <sup>3</sup> )	Mass (g)	Heat Output (W)
$\text{Am}_2\text{O}_3$ tile	1	2.4	11.68	28.03	2.89
Pt cladding	1	0.025	21.45	6.22	
Cu hot shoe	1	0.001	8.96	0.009	
<b>Thermoelectrics</b>					
TAGS	0.25	1.1	6.5	1.79	
PbTe	0.35	1.1	8.16	3.14	
Cu cold shoe	1	0.001	8.96	0.009	
<b>Total</b>		3.53		39.2	

The Sr core thermal output was increased to account for the faster isotope decay, and sized to a 70% thermal output compared to the  $^{238}\text{Pu}$  case at a 15 year-end of life. The cores for both alternate isotope materials were scaled to match the  $^{238}\text{Pu}$  thermal output, though not necessarily the electrical output, as the thermal flux,  $\Delta T$ , heat losses, and equilibrium temperatures were not explicitly simulated for these materials in the PATRAN simulations. In addition, the geometry of the alternate isotopes was not optimized, resulting in fairly tall material stacks rather than the squatter tiles that will give better thermal transport. But this does give a good estimation of the effects of using these other isotopes as the heat sources. The lower thermal output and similar density of the  $^{241}\text{Am}_2\text{O}_3$  results in a 4.8x increase in isotope material mass, and a 14x increase in Pt mass, and an overall 3.5x increase in Core mass. The  $^{90}\text{Sr}$  Core, though having a much higher thermal output than the  $^{241}\text{Am}$  has a comparable mass, primarily due to the 44x increase in Pt needed to capture the penetrating beta particles.

Table 6. The total APPLE thickness and mass for the Pu, Sr, and Am cases, all incorporating the same 5 Wh, 6 layer battery.

APPLE Tile	Area (cm <sup>2</sup> )	Layers	Fill Fraction	Thickness (cm)	Density (g/cm <sup>3</sup> )	Pu Tile mass (g)	Sr Tile mass (g)	Am Tile mass (g)
Power Core x4						44.5	130.0	156.8
Aerogel	100			1.6	0.01	1.6	2.9	3.5
Battery								
Battery layers		6						
Neg. current collector	100	4		0.0013	8.96	4.7	4.7	4.7
LiPON	100	6	0.25	0.0055	2.15	1.8	1.8	1.8
LiCoO <sub>2</sub>	100	6		0.005	4.3	12.9	12.9	12.9
Pos. current collector	100	3		0.0015	2.7	1.2	1.2	1.2
Case	100	2		0.01	1.8	3.6	3.6	3.6
Battery storage (Wh)		5						
Total mass				1.67		70.3	157.1	184.5
Power (W <sub>e</sub> )						1		
Power density (g/W)						70.3	157.1	184.5

This mass difference between isotope cases is reduced, however when incorporated into the full APPLE tile, as the battery size and mass are the same across the isotope designs. As shown in Table 6, adding aerogel, even for the larger stacks when using Sr and Am have a negligible effect on the total mass. And the battery in this specific example is set at 5 Wh for the tile. This represents a charging fraction of 0.5 for the battery over a ten hour period (the rest of the power would be used for mission, avionics, etc.). The battery is composed of 6 anode/cathode layers, for a lithium metal-LiCoO<sub>2</sub> cell shown in Figure 33. The LiPON electrolyte is continuous through the cathode and has an approximate fill fraction across the entire layer of 0.25. The negative current collector is Cu and the positive collectors are Al for this example. This also includes the battery case of a carbon material with the exterior face of this acting as the radiator surface for this design. The total power density of the  $^{238}\text{Pu}$  APPLE tile is 70.3 g/W<sub>e</sub>, including 5 Wh of energy storage per tile. This will enable each tile to supply up to 1 W<sub>e</sub> at all times to the bus without charging the battery, or enable fully charging the attached battery in 5 hours, and any

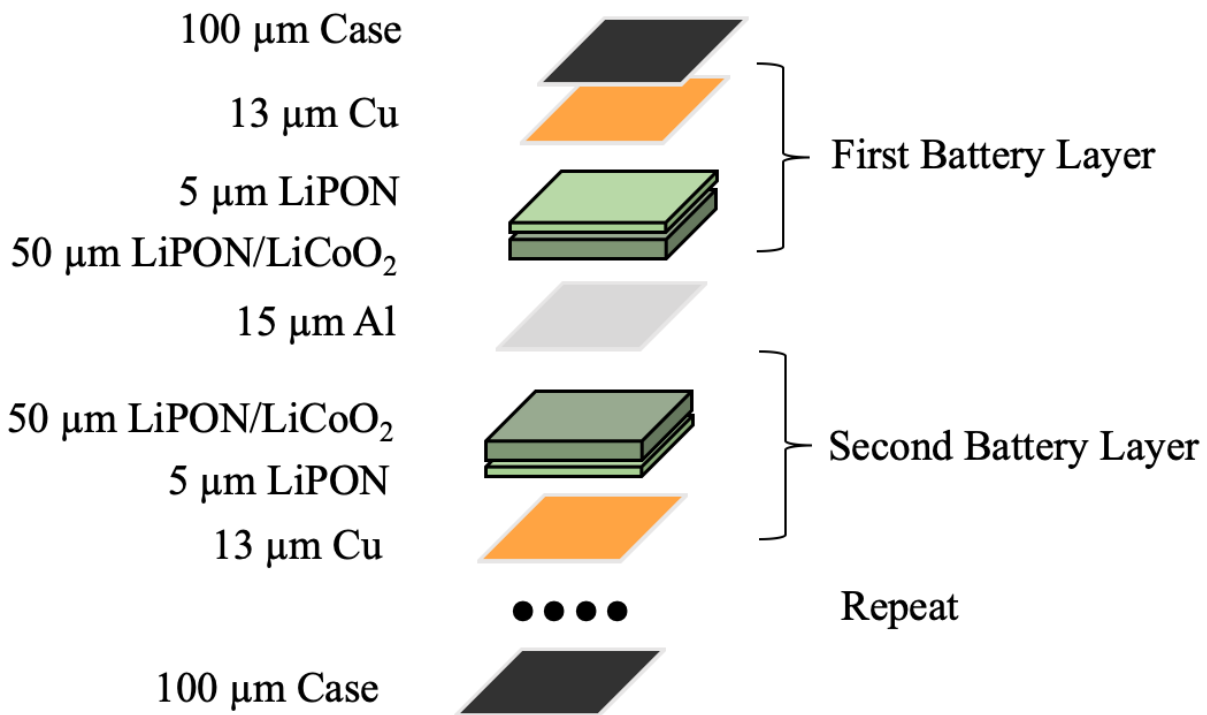


Figure 33. The battery layering for APPLE. This stack can be increased or decreased to meet mission energy storage needs. The bottom case acts as the radiator surface.

combination of operation between. This battery sizing can be adjusted for the mission power profile, either increasing or decreasing the battery storage based on peak power needs.

With this 5 Wh battery, the APPLE tile is 34% battery by mass for the 70.3g/W<sub>e</sub>, however in the extreme case where the battery is removed, the APPLE power density is 47.9 g/W<sub>e</sub> for a more direct comparison to the existing RTG designs that do not incorporate energy storage. This compares very well to the more comparable RTG designs, the MMRTG and the GPHS-RTG, with power densities of 357 g/W<sub>e</sub> and 196 g/W<sub>e</sub> respectively. Thus in a direct comparison

APPLE is 7.5x and 4.1x lighter than the existing alternatives. This is primarily due to the increased radiator efficiency through using the large, multifunctional battery radiator, and through moving the integral carbon aeroshell to the exterior.

In the case for the Sr and Am tiles, the assumption is that they also produce 1 W<sub>e</sub> though as noted before this was not explicitly simulated. These designs are ~2x heavier compared to the Pu case when the onboard energy storage is included.

shows a range of <sup>238</sup>Pu APPLE designs, with variations on the thickness of the isotope core to adjust the heat and electrical output, for a given core footprint of 1cm<sup>2</sup>. The battery size can also be adjusted to meet mission needs depending on how much peak power is needed, changing the APPLE size and power and energy density. This wide range of capabilities is at the heart of the APPLE concept, as a flexible design for mission design and planning.



Table 7. By varying the isotope Core thickness and tailoring the battery size, APPLE designs can be adjusted for any mission.

APPLE Designs	Power ( $W_e$ )	Storage (Wh)	Mass (g)	Specific Power (g/ $W_e$ )	Specific Energy (g/Wh)
<b>0.4 mm</b>					
3 Wh	0.72	3	58.9	81.8	17.7
5 Wh	0.72	5	65.4	90.8	13.1
10 Wh	0.72	10	84.8	118	8.5
<b>0.5 mm</b>					
3 Wh	1.0	3	63.8	63.8	19.1
5 Wh	1.0	5	70.3	70.3	14.1
10 Wh	1.0	10	89.6	89.6	9.0
<b>0.6 mm</b>					
3 Wh	1.2	3	68.7	58.7	20.6
5 Wh	1.2	5	75.1	64.2	15.0
10 Wh	1.2	10	94.5	80.8	9.5

## 6.4. Launch Safety

For environmental protection in the case of a launch failure that would scatter vehicle components into the environment, past RTG designs have used integral aeroshells, typically of carbon, to provide mechanical strength against impact and explosion.<sup>59</sup> Thermal protection in the case of fire was provided in the form of high melting point alloys encasing the isotopes, typically metals like Pt (1,768°C) and Ir (2,446°C). APPLE also uses a Pt material to encase the isotopes for thermal protection, but does not have integral impact protection within the device itself. The carbon aeroshells in the MMRTG and GPHS-RTG designs added considerable mass and volume to those devices, significantly reducing their power densities. While the reliability of launch vehicles has substantially improved in recent decades, catastrophic launch failure for a radioisotope mission still must be mitigated. APPLE intends to use disposable aeroshells for impact protection of the isotopes. This will allow for launch protection mass that can then be discarded after leaving the atmosphere to keep the vehicle transit mass as low as possible. For small vehicle designs, the aeroshells will encase the entire vehicle, with interlocking teeth and be sealed with frangible bolts. This will allow the vehicle safe transit through the atmosphere and allow for the lowest mass during critical vehicle acceleration phases in the mission. For larger missions, the APPLE tiles can be enclosed in aeroshells for disposal.

## 6.5. Spacecraft Cooling Needs

While the thermal simulations in this paper have focused on generating enough heat to keep the battery and spacecraft components warm, during terrestrial portions of the mission, the APPLE heat generation will need to be accounted for. During integration and test, and mission operations while the vehicle is mounted in the fairing up to fairing separation the vehicle will be

surrounded by a large air mass. For integration and test as well as for portions of the mission where the vehicle is in atmosphere, thermal dissipation in atmosphere is actually better than in space. The small size of APPLE and the missions it is meant to support means that heat management in the vehicle fairing when the vehicle is on the launch pad through fairing separation will not be a significant issue. In the case of the SGL mission design, which uses 168 single sided tiles and generates  $2350 W_{th}$  to dissipate, if it were mounted as the sole vehicle in a Falcon 9 fairing, which has an interior volume of  $\sim 650 m^3$ , and a fairing mass of 1900 kg of carbon fiber and aluminum, the temperature of the air and the fairing material would increase by  $1.8 \times 10^{-3} ^\circ C/s$ , or  $\sim 6 ^\circ C/h$ , which does not account for heat losses to the environment. With an approximation of environmental heat losses from convection and radiation at  $11 W/^\circ C m^2$  for the  $\sim 1000 m^2$  fairing surface this means the fairing can comfortably dissipate  $\sim 4x$  the heat generated from the APPLE tiles.

## **6.6. Phase II Project Plan**

In Phase II, APPLE will develop a set of radiation simulations on the APPLE 2.0 battery on radiator design to simulate solar flare, galactic cosmic radiation, and worst case near Jovian environment damage to APPLE components. Work at ORNL will demonstrate radiation test exposure damage and characterization for the battery under simulated mission doses. ORNL will also fabricate 10 x 10 cm radiation hard batteries for characterization and testing. A thermal and mechanical design model will be developed with the objective to provide system and component temperatures and stresses over a mission life based on vehicle and system geometry, thermal generation and transport, emission, and insulation. This model will allow for thermoelectric design and fabrication for the heat conversion component for testing. This thermoelectric design and fabrication will take place in collaboration with JPL's Thermal Energy Conversion Materials Research Group. These thermoelectric devices will be stacked with the radiation hard battery for full stack testing of power generation and energy storage in a thermovac chamber to simulate mission environment. Finally, a candidate power bus design will be developed for the SGL mission, with analysis of how APPLE affects the mission power profile.

## 7. References

---

- <sup>1</sup> MacDonald, Wm., Hughes, G. W., McInnes, C., Lyngiv, A., Falkner, P., Atzei, A., "GeoSail: An Elegant Solar Sail Demonstration Mission," *Journal of Spacecraft and Rockets*, 44, (2007).
- <sup>2</sup> Manzella, D., "Low Cost Electric Propulsion Thruster for Deep Space Robotic Missions," 2007 NASA Science Technology Conference, 2007.
- <sup>3</sup> Landis, G. A., Fincannon, J., "Study of Power Options for Jupiter and Outer Planet Missions," *42<sup>nd</sup> IEEE Photovoltaic Specialists Conference*, New Orleans, LA, June 14-19, 2015.
- <sup>4</sup> Cataldo, R. L., Bennett, G. L., "U.S. Space Radioisotope Power Systems and Applications: Past, Present, and Future," NASA Glenn Research Center (2009).
- <sup>5</sup> Li, H. "Practical Evaluation of Li-Ion Batteries," *Joule*, 3, (2019) pp. 911-914.
- <sup>6</sup> Miller, T. B. "Battery Applications for NASA's Missions - A Historical Perspective," *ARPA-E Robust Affordable Next Generation EV-Storage*, NASA KSC, January 28-29, 2014.
- <sup>7</sup> Zhang, S.S., Xu, K., Jow, T.R., "The low temperature performance of Li-ion batteries," *Journal of Power Sources*, 115, (2003) pp. 137-140.
- <sup>8</sup> Hamon, Y., Douard, A., Sabary, F., Marcel, C., Vinatier, P., Pecquenard, B., Levasseur, A., "Influence of sputtering conditions on ionic conductivity of LiPON thin films," *Solid State Ionics*, 177, 2006, pp. 257-261.
- <sup>9</sup> J. Fu, "Fast Li<sup>+</sup> ion conducting glass-ceramics in the system Li<sub>2</sub>O–Al<sub>2</sub>O<sub>3</sub>–GeO<sub>2</sub>–P<sub>2</sub>O<sub>5</sub>," *Solid State Ionics*, 104 (1997), pp. 191-194.
- <sup>10</sup> Thangadurai, V., Weppner, W., "Li<sub>6</sub>AlLa<sub>2</sub>Ta<sub>2</sub>O<sub>12</sub> (A = Sr, Ba): Novel Garnet-Like Oxides for Fast Lithium Ion Conduction," *Adv. Funct. Mater.*, 15 (2005), pp. 107-112.
- <sup>11</sup> Y. Inaguma, C. Lique, M. Itoh, T. Nakamura, T. Uchida, H. Ikuta, M. Wakihara, "High ionic conductivity in lithium lanthanum titanate," *Solid State Commun.*, 86, (1993), pp. 689-693.
- <sup>12</sup> Kuwano, J., West, A. R., "New Li<sup>+</sup> ion conductors in the system, Li<sub>4</sub>GeO<sub>4</sub>-Li<sub>3</sub>VO<sub>4</sub>," *Mater. Res. Bull.*, 15 (1980), pp. 1661-1667.
- <sup>13</sup> Kanno, R., Murayama, M., "Lithium Ionic Conductor Thio-LISICON: The Li<sub>2</sub>S - GeS<sub>2</sub> - P<sub>2</sub>S<sub>5</sub> System," *J. Electrochem. Soc.*, 148 (2001), pp. A742-A746.
- <sup>14</sup> Plichta, E. J., Henrickson, M., Thompson, R., Au, G., Behl, W. K., Smart, M. C., Ratnakumar, B. V., Suampudi, S., "Development of low temperature Li-ion electrolytes for NASA and DoD applications." *Journal of power sources* 94.2 (2001), pp. 160-162.
- <sup>15</sup> Li, D., Ma, Z., Xu, J., Li, Y., Xie, K., "High temperature property of all-solid-state thin film lithium battery using LiPON electrolyte," *Materials Letters*, 134, (2014) pp. 237-239.
- <sup>16</sup> Mo, S., Lu, P., Ding, F., Xu, Z., Liu, J., Liu, X., Xu, Q., "High-temperature performance of all-solid-state battery assembled with 95(0.7Li<sub>2</sub>S-0.3P<sub>2</sub>S<sub>5</sub>)-5Li<sub>3</sub>PO<sub>4</sub> glass electrolyte," *Solid State Ionics*, 296, (2016) pp. 37-41.
- <sup>17</sup> Wan, J., Xie, J., Kong, X., Liu, Z., Liu, K., Shi, F., Pei, A., Chen, H., Chen, W., Chen, J., Zhang, X., "Ultrathin, Flexible, Solid Polymer Composite Electrolyte Enabled With Aligned Nanoporous Host For Lithium Batteries," *Nature Nanotechnology*, 14 (2019), pp.705-711.
- <sup>18</sup> [www.planetary.org/articles/plutonium-power-for-space-missions](http://www.planetary.org/articles/plutonium-power-for-space-missions)
- <sup>19</sup> Wham, R., Onuschak, B., Sutcliffe, T., "Plutonium-238 Supply project – Additional processing Enabling Power for Future NASA Missions," *Proceedings of 2016 IEEE Aerospace Conference*, Big Sky, Montana, 5-12 Mar 2016.
- <sup>20</sup> ESA Radioisotope Study Final Review – SEA Ltd, 9 February 2021, [www.unoosa.org/pdf/pres/stsc2012/tech-18E.pdf](http://www.unoosa.org/pdf/pres/stsc2012/tech-18E.pdf)
- <sup>21</sup> <https://physics.nist.gov/PhysRefData/Star/Text/ASTAR.html>
- <sup>22</sup> <https://physics.nist.gov/PhysRefData/Star/Text/ESTAR.html>
- <sup>23</sup> <https://physics.nist.gov/PhysRefData/XrayMassCoef/tab3.html>
- <sup>24</sup> Agostinelli, S., Allison, J., Amako, K., Apostolakis, J., Araujo, H., et al., "Geant4: A simulation toolkit," *Nuc. Instr. Phys. Res. A*, 506, (2003), pp. 250-303.
- <sup>25</sup> Ivantchenko, A., Ivantchenko, N., Quesada, Molina, J., Incerti, S., "GEANT4 Hadronic Physics for Space Radiation Environment," *Int J Rad Biol* 88, (2012), pp. 171-175.
- <sup>26</sup> O'Neill, P., Golge, S., Slaba, T., "Badhwar-O'Neill 2014 Galactic Cosmic Ray Flux Model Description," National Aeronautics and Space Administration Report No. NASA-TP-2015-218569, 2015.

- 
- <sup>27</sup> Shea, M., Smart, D., "A Summary of Major Solar Proton Events," *Solar Phys.* 127, (1990) pp. 297-320.
- <sup>28</sup> Cucinotta F., Kim M., Chappell, L., "Space Radiation Cancer Risk Projections and Uncertainties – 2012," National Aeronautics and Space Administration Report No. NASA-TP-2013-217375, 2013.
- <sup>29</sup> ICRP. 2007. The 2007 Recommendations of the International Commission on Radiological Protection. International Commission on Radiological Protection Report No. 103.
- <sup>30</sup> Guttman, D., Woerner, D., "Environmental Requirements Document for Next Generation RTG (Next Gen. RTG)," National Aeronautics and Space Administration Report RPS-REQ-0147 Rev. A, 2020.
- <sup>31</sup> Stoddard, D. H., Albenesis, E. L., "Radiation Properties of <sup>238</sup>Pu Produced for Isotopic Power Generators," Office of Scientific and Technical Information, July 1965.
- <sup>32</sup> Hoefs, J., Sywall, M., "Lithium isotope composition of Quaternary and Tertiary biogene carbonates and a global lithium isotope balance," *Geochimica et Cosmochimica Acta*, 61 (1997), pp. 2679-2690.
- <sup>33</sup> Sedlacek, W. A., Ryan, V. A., "Prompt Activation Analysis for Lithium-6," *Analytical Chemistry*, 40, (1968), pp. 678.
- <sup>34</sup> Barker, F. C., "Neutron and Proton Capture by <sup>6</sup>Li," *Austrian Journal of Physics*, 33, (1980) pp. 159.
- <sup>35</sup> Kim, Y., Veith, G. M., Nanda, J., Unocic, R. R., Chi, M., Dudney, N. J., "High Voltage Stability of LiCoO<sub>2</sub> Particles with a Nano-Scale Lipon Coating," *Electrochimica Acta*, 56, (2011), pp. 6573-6580.
- <sup>36</sup> Xu, F., Dudney, N. J., Veith, G. M., Kim, Y., Erdonmez, C., Lai, W., Chiang, Y.-M., "Properties of Lithium Phosphorus Oxynitride (Lipon) for 3D Solid-State Lithium Batteries," *Journal of Materials Research*, 25, (2010) pp. 1507-1515.
- <sup>37</sup> Caillat, T., "Thermoelectrics: from Space to Terrestrial Applications—Successes, Challenges and Prospects," *College de France, Paris*, March 2013.
- <sup>38</sup> Dustin, J. S., Borrelli, R. A., "Modeling of Am-241 as an alternative fuel source in a radioisotope thermoelectric generator," *Nuclear Engineering and Design*, 385, (2021), pp. 111495.
- <sup>39</sup> Johnson, S. G., "Considerations for Use of Am-241 for Heat Source Material for Radioisotope Power Systems," Idaho National Laboratory, INL/EXT-16-40336-Revision-1.
- <sup>40</sup> Caillat, T., "Thermoelectrics: from Space to Terrestrial Applications—Successes, Challenges and Prospects," *College de France, Paris*, March 2013.
- <sup>41</sup> Fleurial, J.P., Caillat, T., Nesmith, Wm. J., Ewell, R. C., Woerner, D. F., Carr, G. C., Jones, L.E., "Thermoelectrics: From Space Power Systems to Terrestrial Waste Heat Recovery Applications," 2011 Thermoelectrics Applications Workshop, San Diego, California, January 3-6, 2011.
- <sup>42</sup> Caillat, T., "Thermoelectrics: from Space to Terrestrial Applications—Successes, Challenges and Prospects," *College de France, Paris*, March 2013.
- <sup>43</sup> Kim, H. S., Liu, W., Chen, G., Chu, C.-W., Ren, Z., "Thermoelectric Conversion Efficiency," *Proceedings of the National Academy of Sciences*, 112 (2015), pp. 8205-8210.
- <sup>44</sup> Wang, X. Y., Fabanich, W., Schmitz, P., "Advanced Stirling Radioisotope Generator Thermal Power Model in Thermal Desktop SINDA/FLUINT Analyzer," *10th International Energy Conversion Engineering Conference*, 4060, (2012).
- <sup>45</sup> Otting, Wm., Hammel, T., Woerner, D., Fleurial, J.-P., "Advanced Radioisotope Thermoelectric Generator (ARTG) Leverages Segmented Thermoelectric Technology," *NETS 2015*.
- <sup>46</sup> Lu, Z., Li, W., Long, y., Liang, J., Liang, Q., Wu, S., Tao, Y., Weng, Z., Ly, W., Yang, Q.-H., "Constructing a High-Strength Solid Electrolyte Layer by In Vivo Alloying with Aluminum for an Ultrahigh-Rate Lithium Metal Anode," *Adv. Funct. Mater.*, 30, (2020), pp. 1907343.
- <sup>47</sup> Turyshev, S. G., Toth, V. T., "Photometric Imaging With the Solar Gravitational Lens," *Physical Review D*, 101, (2020), pp. 044025.
- <sup>48</sup> Liebes, S., "Gravitational Lenses," *Phys. Rev.* 133, (1964), pp. B835.
- <sup>49</sup> Loureiro, G., Leaney, P. G., "A Systems and Concurrent Engineering Framework for the Integrated Development of Space Products," *Acta Astronautica*, 53, (2003), pp. 945-961.
- <sup>50</sup> <https://gomspace.com/shop/subsystems/power/nanopower-bp4.aspx>
- <sup>51</sup> Appelbaum, J., Landis, G. A., "Photovoltaic arrays for Martian surface power," *Acta Astronautica*, 30, (1993) pp. 127-142.
- <sup>52</sup> <https://solaerotech.com/solaero-makes-history-with-solar-panel-that-powered-first-successful-flight-on-mars/>
- <sup>53</sup> <https://www.linkedin.com/pulse/mars-helicopter-ingenuity-deep-dive-its-6-pack-damien-frost/>
- <sup>54</sup> Yang, J., Caillat, T., "Thermoelectric Materials for Space and Automotive Power Generation," *MRS Bulletin*, 31, (2006), pp. 224–229.
- <sup>55</sup> Emanuelli, E., "NASA Will Pay the Entire Cost of Pu-238 Production," *Space Safety Magazine*, April 24, 2013.
- <sup>56</sup> "ORNL-Produced Plutonium-238 to Help Power Perseverance on Mars." ORNL.gov, July 29, 2020.

---

<sup>57</sup> <https://spacenews.com/dod-looking-for-commercially-available-nuclear-propulsion-for-small-spacecraft/>

<sup>58</sup> Robertson, G.A, Young, D., Love, L., Cunningham, K., Kim, T., Ambrosi, R., M., Williams, H., “Preliminary Analysis: Am-241 RHU/TEG Electric Power Source for Nanosatellites,” *Nuclear and Emerging Technologies for Space 2014*, Stennis, MS, February 24-26, 2014.

<sup>59</sup> Rurerman, J.A., "NASA Historical Data Book Volume VII," U.S. National Aeronautics and Space Administration NASA SP-2009-4012, 2009, p. 741.